Positive muon spin rotation and relaxation measurements on the ferromagnetic superconductor UGe_2 at ambient and high pressure

S. Sakarya,[1] P. C. M. Gubbens,[1] A. Yaouanc,[2] P. Dalmas de Réotier,[2] D. Andreica,[3,4] A. Amato,[3] U. Zimmermann,[3] N. H. van Dijk,[1] E. Brück,[1] Y. Huang,[5] and T. Gortenmulder[5]
[1]*FAME, R3, Faculty of Applied Sciences, Delft University of Technology, 2629JB Delft, The Netherlands*
[2]*CEA/DSM/Institut Nanosciences et Cryogénie, 38054 Grenoble, France*
[3]*Laboratory for Muon-Spin Spectroscopy, Paul Scherrer Institute, 5232 Villigen-PSI, Switzerland*
[4]*Faculty of Physics, Babes-Bolyai University, 400084 Cluj-Napoca, Romania*
[5]*van der Waals-Zeeman Laboratorium, Universiteit van Amsterdam, 1018XE Amsterdam, The Netherlands*
(Received 4 August 2009; revised manuscript received 17 December 2009; published 29 January 2010)

Results of a detailed investigation of the ferromagnetic superconductor UGe_2 using positive muon spin rotation and relaxation techniques are presented. The pressure and temperature dependences of the frequencies and related spin-spin relaxation rates show that the transition from the weakly to the strongly polarized magnetic (WP-SP) phases is still observable at $T_X \simeq 3$ K under a pressure of 1.33(2) GPa. Thus this transition survives at higher pressures than previously believed. The temperature T_X at 1.00(2) GPa corresponds to a thermodynamic phase transition rather than a crossover. No such statement can be given reliably at lower pressure. A substantial shrinking of the component along the easy axis of the diagonal hyperfine tensor, at the muon site where it is large, is observed in the SP phase relative to the WP phase. This corresponds to an appreciable decrease in the electronic density at the Fermi level in the SP phase. The investigation of the paramagnetic-ferromagnetic critical spin dynamics at ambient pressure and at 0.95(2) GPa shows that the simple one-band model is an oversimplification inconsistent with our critical spin-dynamics results. Data from specific heat, Fermi-surface studies, Hall effect, neutron form factor, and spectroscopic techniques supports this conclusion. Even at 0.95(2) GPa the conduction electrons are characterized by a small magnetic moment, relative to the bulk magnetization per uranium atom.

DOI: 10.1103/PhysRevB.81.024429 PACS number(s): 74.25.Ha, 74.70.Tx, 76.75.+i

I. INTRODUCTION

The discovery of superconductivity in the ferromagnetic binary compound UGe_2 at low temperature and within a limited pressure range, in which the Curie temperature T_C is tuned to zero,[1] has raised the possibility that the same $5f$ electrons are at the origin of both the ferromagnetism and superconductivity of the compound. Since superconductivity is a property of the conduction electrons, the $5f$ electrons would be fully itinerant. In this simple model, ferromagnetism would arise from the splitting of the conduction band by the spontaneous molecular field below T_C.

This simple electronic picture may not be valid as suggested by the observation of a complex Fermi surface which consists of multiple-connected cylindrical and ellipsoidal sheets.[2] In addition, UGe_2 is certainly not a simple ferromagnet since it exhibits two ferromagnetic phases.[3] In fact, as first deduced from positive muon spin relaxation measurements of the critical spin dynamics at ambient pressure,[4] UGe_2 should be viewed as an electronic system with coexisting $5f$ localized states and itinerant states.

Here we report on extensive positive muon spin rotation and relaxation (μSR) studies performed on single crystals under pressure. These techniques probe the magnetic properties of magnetic materials through the dipolar and hyperfine couplings of the muon spin to the magnetic density of the compound under investigation. Because the muon localizes in an interstitial site, rather than at a substitutional site, in favorable cases one may access to the magnetic properties of the conduction electrons.

Our study allows us to extract information about the electronic states at the Fermi level and to characterize the magnetic transitions between the paramagnetic and ferromagnetic states and between the two ferromagnetic states. In addition, we show that the study of the spin dynamics under a pressure of 0.95(2) GPa still reveals an electronic component with a small magnetic moment.

The organization of this paper is as follows. Section II summarizes the physical properties of UGe_2 related to our work. In Sec. III we describe the samples probed by the measurements and the two spectrometers used for this study. We pay particular attention to the high-pressure measurements. Section IV presents our experimental results. Their meaning is also discussed in this section. We start by the temperature and pressure dependences of the spontaneously precessing signal. This is followed by the temperature and pressure dependence of the related spin-spin relaxation rates. Then we focus on the spin-lattice relaxation rate at 0.95(2) GPa and compare to the results at ambient pressure. The summary of our key results is given in Sec. V. In the same section we compare the electronic structure of UGe_2 and other actinide compounds. Rather than a conclusion section, the last section (Sec. VI) proposes μSR experiments to be performed to increase our understanding of the physics of UGe_2. Informations related to the μSR technique are provided in two Appendices. In Appendix A the minimum theoretical background required to analyze the μSR data is given. We complete our paper by an extended discussion of the two muon localization sites in Appendix B. This allows us to get information on their coupling constants.

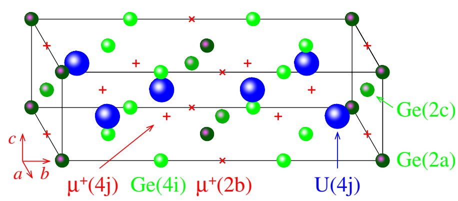

FIG. 1. (Color online) The orthorhombic crystallographic structure of UGe_2. The uranium atoms are pictured with large spheres and germanium atoms with smaller ones. The figure shows the unit cell of UGe_2 containing four formula units. The two muon stopping sites are indicated by + and × symbols. One of three coordinates of the muon position 4j is unknown. In the figure we have chosen the position at the center of a tetrahedron which is formed by two uranium atoms and two germanium atoms at position 4i.

II. SOME PHYSICAL PROPERTIES OF UGe_2

Here we summarize the physical information available for UGe_2 relevant for our study. The compound crystallizes in the orthorhombic $ZrGa_2$-type structure (space group *Cmmm*).[5,6] Its unit cell, with dimensions[5] $a=4.036$ Å, $b=14.928$ Å, and $c=4.116$ Å, contains four formula units. Two free parameters are required to describe the crystal structure. The uranium atoms are at position 4j of relative coordinates $(0,y,\frac{1}{2})$ with $y=0.1415$. Germanium atoms located at position 4i have relative coordinates $(0,y,0)$ with $y=0.3084$. The other germanium atoms are at two positions, i.e., 2a and 2c, of relative coordinates (0,0,0) and $(\frac{1}{2},0,\frac{1}{2})$, respectively. The structure is shown in Fig. 1. The U atoms are arranged in zigzag chains of nearest neighbors in the **a** direction. The nearest-neighbor uranium distance $d_{\mathrm{U-U}}$ is equal to $d_{\mathrm{U-U}}\approx 3.82$ Å at zero pressure but is possibly reduced to about 3.5 Å at 1.3 GPa due to a slight flattening of the chains.[7] This would compare well with the Hill limit of 3.5 Å.[8]

The ferromagnetic order at ambient pressure is found below $T_C=52$ K. The magnetic moment is directed along the **a** axis with a saturation value of $m_{\mathrm{U}}^a=1.4\mu_B/\mathrm{U}$.[9] Magnetic measurements indicate a very strong magnetocrystalline anisotropy[10] with **a** being the easy axis. T_C is reduced for increasing pressure and finally vanishes at a pressure of $p_c \simeq 1.6$ GPa. The phase transition from the paramagnetic to the ordered state is second order up to $p_c^* \simeq 1.2$ GPa and becomes first order at higher pressure.[11,12] Within the ferromagnetic phase, a second transition occurs. At ambient pressure it takes place at $T_X\approx 30$ K but its physical signatures are not pronounced. As the pressure is increased, T_X decreases and the transition itself gets better observable. Specific-heat measurements suggest that a thermodynamic phase transition occurs at T_X, at least under a pressure slightly below p_c^*.[13] It is believed that $T_X=0$ at p_c^*. Below T_X the uranium magnetic moment is enhanced and therefore the temperature region between T_C and T_X was named the weakly polarized (WP) phase whereas the lower temperature region $T<T_X$ was coined the strongly polarized (SP) phase.[14] It has been suggested theoretically that T_X could be related to the formation of a simultaneous charge and spin-density wave.[15] No experimental signature of such a wave has ever been published.

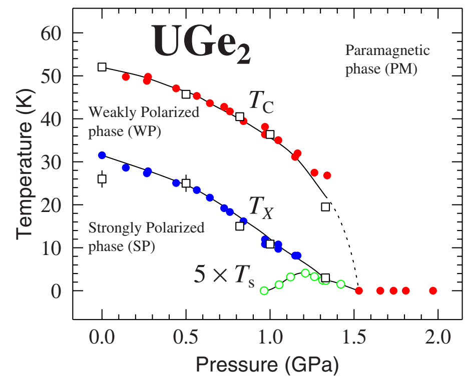

FIG. 2. (Color online) The temperature (T) versus pressure (p) phase diagram of UGe_2 established from various measurements. Below the Curie temperature T_C there are two ferromagnetic phases, a WP phase and a SP phase. The transition temperature between these two phases is denoted T_X. For clarity the superconducting region between 1.0 and 1.6 GPa indicated by open circle is exaggerated. With open squares we indicate T_C and T_X values as determined by the μSR experiments presented in this work. The solid and dotted lines are guides to the eye. Figure adapted from Ref. 19.

Superconductivity is found in a limited pressure range between 1.0 and 1.6 GPa with a maximum transition temperature ≈ 0.7 K around p_c^*. In this pressure range, the magnetic moment is still appreciable $(1\mu_B/\mathrm{U})$. Superconductivity is believed to be related to the vanishing of T_X.

The pressure dependence of the transition temperature T_C from the paramagnetic state (PM) to the WP state, the transition temperature within the ferromagnetic state T_X, and the superconducting transition temperature T_s, are all shown in Fig. 2. The data points were obtained from measurements with various techniques.[1,3,11,16–18]

For an insight into the mechanism of the electronic pairing in the superconducting state of UGe_2, information on its electronic properties is essential. UGe_2 at low temperature is believed to be a Fermi-liquid system because its specific heat varies linearly with temperature. Actually, it is classified as a heavy fermion compound since its Sommerfeld coefficient is pretty large at ambient pressure: $\gamma=30$ mJ/(K^2 mol).[20] The γ value is only slightly pressure dependent up to about 1.0 GPa where it displays an upturn. It reaches $\gamma \simeq 100$ mJ/(K^2 mol) at 1.4 GPa. In agreement with the Fermi-liquid behavior observed by the specific heat, the electrical resistivity ρ at low temperatures follows a temperature dependence $\rho(T)=\rho_0+AT^2$. Under pressure, the coefficient A increases steeply above 1.0 GPa, and has a maximum in the range 1.3–1.4 GPa.[1,20] That the parameters γ and A display a maximum at about the same pressure is not surprising for a Fermi-liquid system since one expects A to be proportional to γ^2. This is the Kadowaki-Woods relation which is obeyed for UGe_2 with a ratio $A/\gamma^2\simeq 10$ $\mu\Omega$ cm mol^2 K^2 J^{-2} up to $\sim$1.3 GPa. This is the expected ratio value for heavy fermion compounds; see the recent discussion of Ref. 21. Both measurements point out to a maximum of the conduction-electron density in the range 1.3–1.4 GPa.

De Haas-van Alphen (dHvA) effect measurements support the existence of a maximum in the electron density at intermediate pressure.[22] Denoting m_e the free electron mass, the mass associated with a large orbit, β, being $12m_e$ at ambient pressure, gradually increases to $16m_e$ at 1.22 GPa, and then suddenly jumps to $39m_e$ at 1.32 GPa. In addition, a discontinuous change in the Fermi surface occurs across p_c. Open electronic orbits have been inferred from transverse magnetoresistance.[2] A discussion of the large cyclotron effective masses show that the $5f$ electrons cannot be considered as fully localized since the Fermi surfaces are nonsimilar to those of non-$5f$ Th compounds.[2] It does not seem either to fall in the class of Kondo-lattice compounds because extreme large masses in the range of $100m_e$ or above are not detected.[2] An $5f$-itinerant picture is also not appropriate as the data discussed below indicate. We note that the magnetization data cannot be taken as a proof of the itinerant nature of the $5f$ electrons.[12] In fact, the Fermi surface is complicated and consist of multiple-connected large cylindrical sheets and ellipsoidal closed ones.[2] Therefore it may not be surprising that a simple one-band model which would split in the ferromagnetic state is an oversimplification. The data discussed below support the schematic of two electronic subsets.

Hall coefficient measurements at ambient pressure exhibit a sudden increase in the carrier concentration below T_X.[23] The Hall data support the view of the existence of two electron subsets differing by their localization character.

A finite ratio of $\lim_{T\to 0} C/T$ is found in the superconducting region.[13] A similar behavior of the specific heat has been reported for UPd_2Al_3 (Ref. 24) which is also a heavy fermion superconductor but which displays an antiferromagnetic phase transition at low temperature rather a ferromagnetic transition as UGe_2. The finite ratio was interpreted as a signature of a two $5f$ electron subsets; one responsible for the antiferromagnetic state and one exhibiting superconductivity at low temperatures. Such a picture was confirmed later on by μSR measurements[25] and found consistent with the results of an NMR study.[26]

There is interest to discuss together the bulk magnetization and neutron form factor data. The measurement of the latter physical quantity allows one to estimate the localized magnetic moments, i.e., the localized uranium magnetic moment in our case. The difference between the magnetic moment per uranium atom deduced from the bulk magnetization and the neutron-estimated localized moment is conventionally attributed to the diffuse component which we take to arise from the conduction electrons. This allows to infer the conduction-electron magnetic moment, $m_{\rm cond}$. Form factor studies are available at ambient pressure and 1.4 GPa for $T \ll T_C$.[9,27] They provide a really small value at ambient pressure: $m_{\rm cond}=0.04(3)\mu_B$. Interpolating the bulk magnetization data, $m_U^a \simeq 0.91\mu_B$ at 1.4 GPa,[11] and using the neutron result, one gets $m_{\rm cond}\simeq 0.2\mu_B$ at 1.4 GPa. Interestingly, $m_{\rm cond}$ and m_U^a are found antiparallel at that pressure. We therefore conclude that pressure increases substantially $m_{\rm cond}$, at least at 1.4 GPa. Note that $m_{\rm cond}$ is appreciable in the pressure range where the conduction-electron density exhibits a maximum. In the framework of the Stoner model $m_{\rm cond}$ is attributed to the spontaneous splitting of the conduction bands. It is difficult to relate the size of $m_{\rm cond}$ to the conduction-electron properties. However, a large electronic density at the Fermi level favors the appearance of an appreciable $m_{\rm cond}$ value; see, for example, Ref. 28.

Studies designed to probe the electronic $5f$ correlations have been reported: x-ray photoemission spectroscopy,[29] Bremsstrahlung isochromat spectroscopy,[29] electron-positron momentum density,[30] and x-ray absorption and magnetic circular dichroism at the $M_{4,5}$ edges of uranium.[31] An interpretation of all these data, as well as the angular dependence of the frequencies of dHvA oscillations, cannot be achieved assuming fully itinerant $5f$ states.[31] A local spin-density approximation (LSDA) computation supplemented by a strong $5f$ Coulomb repulsion, the so-called LSDA+U method, provides a qualitative understanding of the data choosing U $=2$ eV. This is larger than the commonly assumed value of ~ 0.7 eV.[32]

Hence, the complexity of the Fermi surface, the Hall-effect measurements as well as the observed finite ratio of C/T in the superconducting region and the small value of the conduction-electron magnetic moment deduced from the analysis of the neutron form factor, all these experimental results indicate that the model of a single $5f$-band model spontaneously split in the ferromagnetic state is not appropriate. In addition, the analysis of spectroscopic data shows that the electronic correlations in UGe_2 are particularly strong. All these results support the schematic of a two electronic subsets system originally put forward from the study of the critical spin dynamics at ambient pressure by μSR.[4]

III. EXPERIMENTAL

Two different crystals were prepared for the measurements. Both of them were grown from polycrystalline ingots using a Czochralski tri-arc technique. One of them, referred to as "crystal A" in the following, was annealed at 800 °C for one week. No heat treatment was done for crystal B. It is that sample which was used in the first published μSR work.[4] Since we did not characterize our sample under pressure at low temperature we could not determine whether it exhibits superconductivity. Hence, we did not attempt to study the superconducting phase using the μSR techniques.

A cylinder with 5 mm diameter and of a length of 19.5 mm was cut from single crystal A. The cylinder axis was parallel to **a**, i.e., the easy magnetic axis. Subsequently, a sphere with a diameter of 4.5 mm and a cylinder of diameter 4.3 mm and length 13.5 mm were cut from the original cylinder. Crystal B was cut in slices in such a way as to produce two disk-shape mosaic samples. They differ by the orientation (either parallel or perpendicular) of **a** relative to the normal to the sample plane. The μSR techniques are presented in Refs. 33 and 34.

Measurements at ambient pressure were performed with the cylinders and the disk-shape samples at the general purpose surface-muon (GPS) spectrometer of the Swiss muon Source (SμS) located at the Paul Scherrer Institute (PSI, Villigen, Switzerland). Transverse-field measurements designed to measure the paramagnetic frequency shift were done with the sphere at GPS. The sphere was rotated *in situ* with $\mathbf{S}_\mu$ perpendicular to the rotation axis. The external magnetic field $\mathbf{B}_{\rm ext}$ was applied perpendicular to both $\mathbf{S}_\mu$ and the

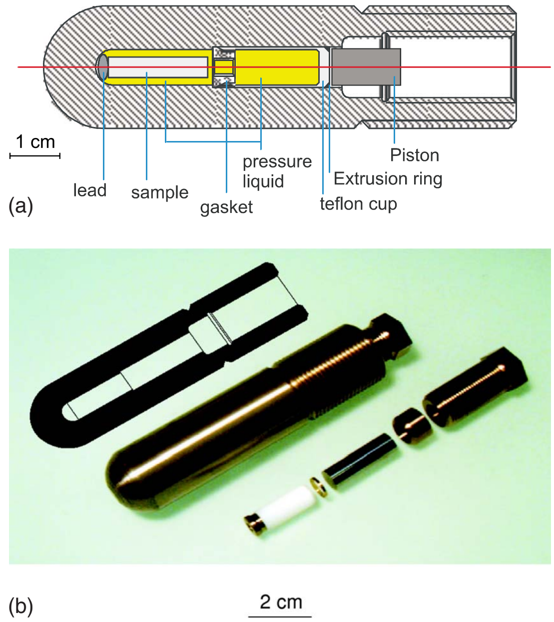

FIG. 3. (Color online) The μSR pressure cell. (a) schematic overview of the cell. The different parts are indicated. For details, see the main text. (b) photograph of different parts of the cell.

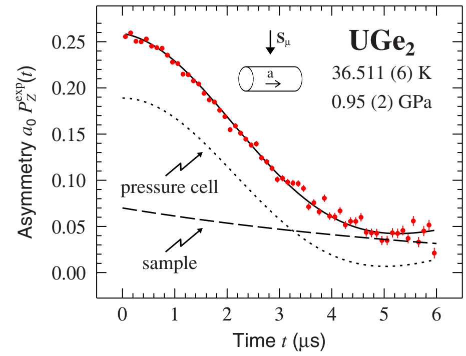

FIG. 4. (Color online) UGe_2 spectrum recorded in zero field under a pressure of 0.95(2) GPa at 36.511(6) K. The corresponding reduced temperature is $\tau \equiv (T-T_C)/T_C = 0.0007(3)$. The sample is a single-crystalline cylinder whose **a** axis, i.e., the easy axis, is oriented perpendicular to the initial muon beam polarization. The full line is a fit to a weighted sum of two components, accounting, respectively, for the response of the sample—exponential function, dashed line—and of the pressure cell—Kubo-Toyabe function, Eq. (2)—dotted line. The initial asymmetry related to the sample is only about 0.07 for this spectrum rather than 0.010 for most measurements under pressure, see Fig. 6. This simply reflects the fact that the zero-field critical spin dynamics investigation was carried out after the high-pressure measurements (above 1.0 GPa). The diameter of the cylinder had to be reduced for the high-pressure measurements.

rotation axis. All these measurements cover the temperature range from 5 to 200 K using standard ^{4}He cryostats.

The number of detected positrons at time t, denoted as $N(t)$, is simply related to the asymmetry $a_0 P_\alpha^{\exp}(t)$ ($\alpha = X$ or Z)

$$N(t)/N_0 = \exp(-t/\tau_\mu)[1 + a_0 P_\alpha^{\exp}(t)] + b_{\rm el}. \quad (1)$$

The constant N_0 gives the scale of the counting, τ_μ is the muon lifetime, a_0 the initial asymmetry, $P_\alpha^{\exp}(t)$ the polarization function of interest and $b_{\rm el}$ measures the electronic background contribution. It can be time independent as at GPS or might contain some contributions of the accelerator frequencies, which are well known and can be safely taken into account in the analysis. This is the case for the general purpose decay-channel (GPD) spectrometer of PSI, which is the spectrometer we choose for the high-pressure studies. For that instrument, high-energy muons (with an impulse of 105 MeV/c) are used. A large amount of such muons probes the sample even if it is in a bulky environment such as a pressure cell.

Let us focus on the measurements at GPD. The pressure cell was attached to the cold finger of a ^{4}He or ^{3}He cryostat. The low-pressure measurements were performed mostly with the cylinder with the larger diameter. However, to reach pressures higher than 1.0 GPa, the smaller sample cylinder had to be used. Because of the history of our studies, the investigations of the spin dynamics were performed with the smaller cylinder, despite the pressure range which was slightly below 1.0 GPa. The pressure cells are made of nonmagnetic copper beryllium and a typical schematic overview is shown on Fig. 3.

Even though teflon gives quite a large μSR signal[35,36] a cup made of this material was used in combination with a gasket in order to prevent leakage of the pressure liquid. However such arrangement is kept away from the sample space and therefore the muon beam.[35] Consequently solely the Cu-Be pressure cell contributes to the μSR background signal. Note that such background μSR signal is included in the $a_0 P_\alpha^{\exp}(t)$ term of Eq. (1) and should not be confused with the contribution $b_{\rm el}$. Such μSR background signal created by the pressure cell is well described, at low temperatures, by the Kubo-Toyabe relaxation function

$$P_{\rm KT}(t) = \frac{1}{3} + \frac{2}{3}(1 - \Delta_{\rm G}^2 t^2)\exp\left(-\frac{1}{2}\Delta_{\rm G}^2 t^2\right). \quad (2)$$

It has its origin in static magnetic fields with a Gaussian field distribution of width $\Delta_{\rm G}/\gamma_\mu$, where γ_μ is the muon gyromagnetic ratio ($\gamma_\mu = 851.615$ Mrad s^{-1} T^{-1}). The static magnetic field comes from the nuclear magnetic moments of ^{63}Cu, ^{65}Cu, and ^{9}Be in the copper-beryllium alloy. Below 40 K, $\Delta_{\rm G}$ is temperature independent and equal to 0.345(2) μs^{-1} (for further details, see Ref. 35).

An example of a measurement in zero field performed with the pressure cell is presented in Fig. 4. Because the spectrum does not display oscillations from the sample and the relaxation is not strong, a high binning of the data is possible. The asymmetry has been deduced from the positron counts using Eq. (1). Although the contribution of the cell to the measured signal is important it is still possible to get a very reliable μSR spectrum from the sample. The figure displays a spectrum recorded with the most difficult experimental conditions, i.e., the relaxation of the μSR signal from the sample is weak and the sample is small. As shown later in Fig. 6, it is quite easy to obtain a good quality oscillating μSR signal from a sample in the cell.

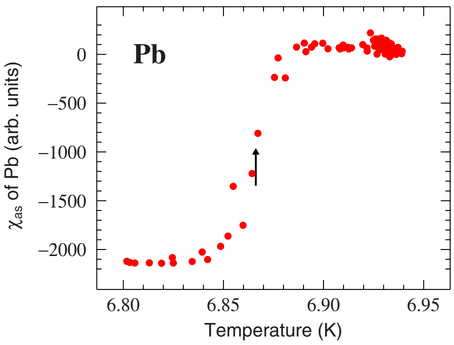

FIG. 5. (Color online) The pressure inside the pressure cell is estimated by measuring the ac susceptibility of a piece of lead located at the bottom of the pressure cell, just below the sample (see Fig. 3 and the main text). From this plot we determine p =0.92(2) GPa.

For each applied pressure, we determine the pressure inside the cell by measuring the ac susceptibility, χ_{ac}, as a function of temperature of a piece of lead which is fixed to the bottom of the pressure cell. Note that we do not rely on any calibration or interpolation for the pressure inside the cell. An example of the pressure determination can be seen in Fig. 5. χ_{ac} shows a sharp drop as soon as lead gets superconducting. Here the superconducting transition temperature T_s, which determines the pressure p by the formula $T_s(p) = T_s(0) - 0.364 \times p$ (Ref. 37) with T_s in K, p in GPa and $T_s(0) = 7.204$ K, is defined as the midpoint of this drop. The temperature $T_s(0)$ was measured with our experimental setup. We estimate the uncertainty to be ± 20 MPa for each of the measured pressure in this report.

IV. PRESENTATION OF THE EXPERIMENTAL RESULTS AND DISCUSSION OF THEIR MEANING

A. Preliminaries

Two muon sites are detected in UGe_2. A complete study using Knight shift measurements in the paramagnetic-state and zero-field measurements in the magnetically ordered state at low temperature, both at ambient pressure, is presented in Appendix B. The two muon positions denoted as 2b and 4j (Wyckoff notation) are graphically localized in the crystal structure displayed in Fig. 1. The hyperfine constants are listed in Table V. While the site at position 2b is completely determined, the muon site at position 4j is characterized by a free coordinate which is unknown. The muon position 4j shown in Fig. 1 assumes the muon to be at the center of a tetrahedron. The uncertainty in the muon localization does not impede the analysis of the data given below. The key feature to remember about the two muon sites is that the component along the easy axis of the diagonal hyperfine tensor is quite small at position 2b relative to the same component at position 4j. This implies that the muon is far more sensitive to the conduction electron density in the latter site than in the former one.

One could be doubtful of the possibility to detect two spontaneous frequencies from a sample sitting in the pressure cell. Figure 6 shows clearly that it is in fact quite easy.

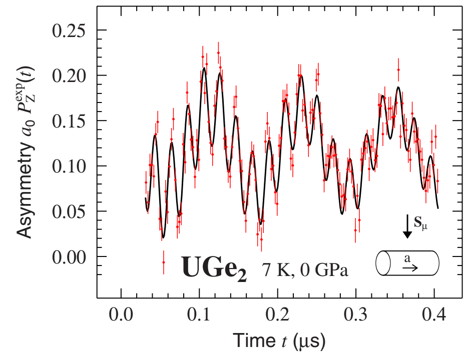

FIG. 6. (Color online) Example of a zero-field spectrum recorded for a sample in the pressure cell at ambient pressure and at low temperature with $\mathbf{S}_\mu \perp \mathbf{a}$. The spectrum was recorded with the larger cylinder at the GPD spectrometer. The beating of the two frequencies arising from the sample is clearly observed. The initial asymmetry from the sample is ~0.10. This is about half of the value for the similar spectrum shown at Fig. 19. This is easily seen graphically: while the oscillations of the present spectrum cover an asymmetry range of ~0.20, this range is twice as much for the spectrum recorded without the pressure cell.

Because of the large contribution of the cell to the measured asymmetry, the spectrum is noisier but it compares favorably with a similar spectrum recorded with no pressure cell as the oscillating spectrum displayed in Fig. 19.

The measurement of the frequencies at low temperature as a function of pressure enables us to get information within our experimental conditions (sample and pressure quality) on the pressure at which the magnetic phase transition changes from second order to first order, as the pressure is increased. In Fig. 7 we display the two local muon fields at low temperature versus pressure. The two pressure dependences are smooth up to at least 1.0 GPa. Since we have not recorded any data points between 1.0 and 1.25 GPa, we cannot determine whether the local fields display a break in their pressure dependence at $p_c^* \simeq 1.2$ GPa, as it was found for the magnetization.[11] Anyhow, the key feature of the data of Fig. 7 to remember is that, within our experimental conditions, the paramagnetic/ferromagnetic transition is certainly second

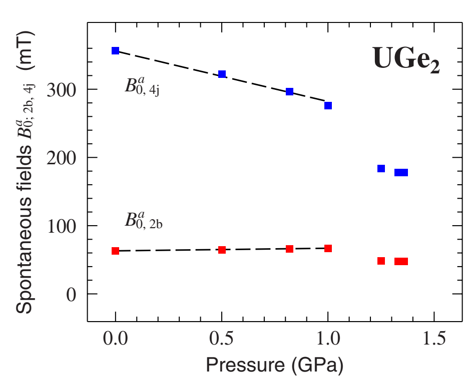

FIG. 7. (Color online) The two spontaneous fields, $B^a_{0,2b}$ and $B^a_{0,4j}$, as a function of pressure. The measurements were performed at about 5 K, except at ambient pressure for which the temperature was 7.0 K. The dashed lines result from linear fits for pressure up to 1.0 GPa.

order up to 1.0 GPa. This will be important when discussing the spin-lattice relaxation in Sec. IV C.

B. Spontaneous frequencies and related relaxation rates versus temperature and pressure

Here we discuss spectra recorded with the GPD instrument in zero field for $T < T_C$: $a_0 P_Z^{\mathrm{exp}}(t)$ is measured. Wiggles are observed because we probe the magnetically ordered state. The asymmetry is made of the weighted sum of three components, two from the sample (we recall that the muon has two localization sites) and one from the pressure cell

$$a_0 P_Z^{\mathrm{exp}}(t) = \sum_{i=1}^{2} a_i \exp(-\lambda_{X,i} t)\cos(2\pi\nu_i t - \psi) + a_{\mathrm{KT}} P_{\mathrm{KT}}(t). \tag{3}$$

A relaxation rate is denoted as $\lambda_{X,i}$ since it describes the damping of the oscillations arising from the muon spin precession around a spontaneous field. It is important to note that the sum of the sample asymmetry, i.e., $a_1 + a_2$, is a measure of the magnetic volume in the sample. The sample volume is fully magnetic if this sum is equal to the value of the initial asymmetry observed in the paramagnetic state. We shall first focus our attention to the data recorded up to 1.0 GPa.

1. Low-pressure results

In Fig. 8 the two measured spontaneous fields and associated relaxation rates are shown as a function of temperature for four pressures (including ambient pressure) up to 1.0 GPa. The thermal behavior of the fields as the sample is warmed toward T_C is smooth as expected for a second-order phase transition. This is entirely consistent with the results presented in Fig. 7.

An anomalous thermal behavior is observed for the four quantities at 1.00(2) GPa. For example, it manifests itself as a pronounced peak in $\lambda_{X,2b}(T)$ and $\lambda_{X,4j}(T)$ around 11 K. An indication of such a peak around 15 K is already present in the $\lambda_{X,4j}(T)$ data at 0.82 GPa. An anomaly in the form of a bump is detected at the other two pressures for $\lambda_{X,4j}(T)$. We have reported in Fig. 2 the positions of the detected anomalies from our study. They clearly correspond to a signature of T_X. We have also indicated T_C values as defined by the vanishing of the frequencies at the phase transition. Our determinations of T_X and T_C are consistent with published results.

The relaxation rate λ_X probes the magnetic fluctuations of the field at the muon site along the spontaneous field direction, i.e., along **a**. This means that these fluctuations display a well-defined peak around T_X at 1.00(2) GPa. This suggests that T_X corresponds to a thermodynamic transition at 1.00(2) GPa rather than a crossover. An inspection of the $\lambda_{X,i}(T)$ data at Fig. 8 indicates that the rates are similar outside the critical regions at T_X and T_C. This means that the field distributions along the two spontaneous fields for the WP and SP phases are qualitatively the same.

We shall now focus on the spontaneous field data, looking for possible relations between the fields and the bulk magnetization data. We present in Fig. 9 the normalized spontaneous fields for two pressures and compare to the normalized magnetization.

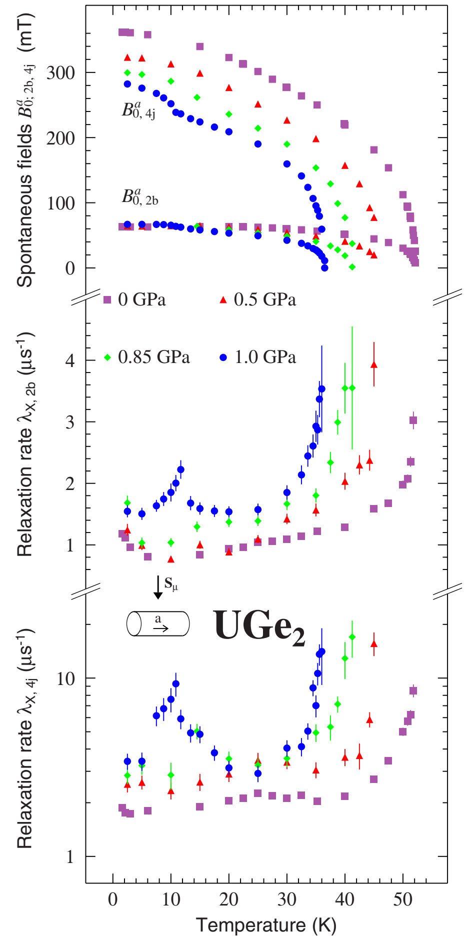

FIG. 8. (Color online) The two spontaneous fields, $B^a_{0,2b}$ and $B^a_{0,4j}$, and associated spin-spin relaxation rates, $\lambda_{X,2b}$ and $\lambda_{X,4j}$, as a function of temperature at four pressures up to 1.0 GPa in UGe_2. As always found in this study, the asymmetry for the muon at position 2b is slightly larger than at position 4j. The uncertainty for each of the pressure is ± 20 MPa.

According to Eq. (A3), the normalized spontaneous field should track the normalized magnetization. However, it is well known that this is not always strictly observed even for simple metals such as Fe, Ni, and Co.[38,39] This has been attributed to the effect of the zero-point motion of the muon on the effectively measured hyperfine field.[40] In addition, because we do not expect the muon wave function to be spherically symmetric, in particular, at position 4j, the measured dipole field may also be influenced by the zero-point motion of the muon.[41] We note that at ambient pressure the deviation from the behavior predicted by Eq. (A3) is larger for the muon at position 4j, which is characterized by a larger hyperfine coupling constant $\mathfrak{H}^{b^\perp}_{4j}$ and a geometry which deviates strongly from the spherical symmetry. The deviation from proportionality gets smaller as the pressure is increased. This suggests that $\mathfrak{H}^{b^\perp}_{4j}$ decreases under pressure. We postpone further discussion of this possible effect after the presentation of Fig. 11.

It is remarkable that the value of the normalized magnetization is always intermediate between the values of the two

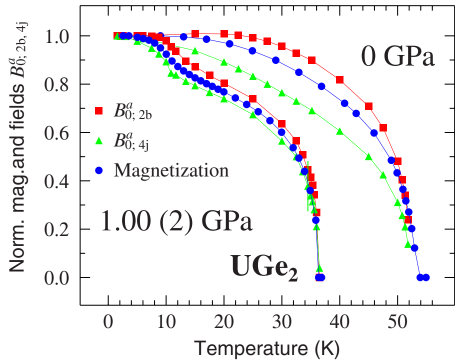

FIG. 9. (Color online) Examples of normalized spontaneous fields (deduced from Fig. 8) and normalized magnetization from Ref. 11 versus temperature. For simplicity we plot the data for only two pressures. The behavior of the data at 0.50(2) and 0.85(2) GPa is obviously intermediate. The normalizations have been done with the lowest measured points. The lines simply link the symbols. The figure shows, as expected, that the spontaneous fields do not track the bulk magnetization at any pressures. As the pressure increases the deviation from proportionality of the spontaneous fields and magnetization gets smaller.

normalized spontaneous fields for a given muon site as illustrated in Fig. 9. This suggests to consider the mean of the two normalized fields

$$M_{\rm nf}(T) = \frac{1}{a_{2b}+a_{4j}} \times \left[a_{2b}\frac{B^a_{0,2b}(T)}{B^a_{0,2b}(T=0)} + a_{4j}\frac{B^a_{0,4j}(T)}{B^a_{0,4j}(T=0)} \right]. \quad (4)$$

In Fig. 10 we compare $M_{\rm nf}$ and the normalized magnetization versus temperature.

The empirical relation in Eq. (4) provides an incredible good description of the data, except at ambient pressure. This is obviously consistent with the plots in Fig. 9. This means that the muon zero-point motion has an effect opposite, but

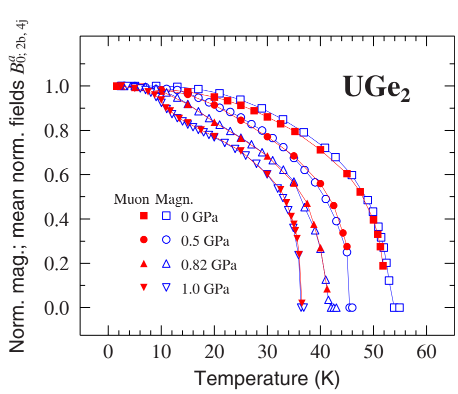

FIG. 10. (Color online) Normalized spontaneous fields (deduced from Fig. 8) averaged over the two observed muon sites (filled symbols) and normalized magnetization (open symbols) from Ref. 11 versus temperature at four pressures up to 1.0 GPa. The uncertainty for each of the pressure is ± 20 MPa. The data have been normalized to the lowest temperature measured. The lines simply link the symbols. The figure illustrates the fact that $M_{\rm nf}(T)$ tracks the bulk magnetization to a good approximation.

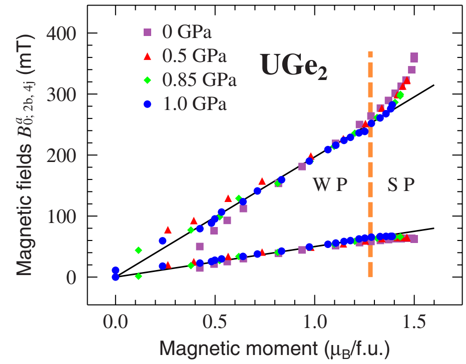

FIG. 11. (Color online) Spontaneous fields (deduced from Fig. 8) versus the magnetic moment per formula unit $m^a_{\rm U}$ (from Ref. 11) for four pressures up to 1 GPa. We specify the two magnetic phases in the ferromagnetic region: the SP and WP phases as deduced from the data of Fig. 2 and Ref. 11. The vertical dashed line separates the two phases. The line is justified because the SP phase occurs at a given value of the ordered moment (Ref. 11). The two solid lines results from linear fits with slopes equal to 50 mT/μ_B and 197 mT/μ_B. The uncertainty for each of the pressure is ± 20 MPa.

of the same amplitude, on the coupling constants for the two muon sites. A detailed modeling of the muon wave function is beyond the scope of this paper but is required to fully understand such an observation.

Instead of plotting a quantity proportional to B^a_i versus temperature, according to Eq. (A3), it seems wiser to consider B^a_i versus $m^a_{\rm U}$, the temperature (and the pressure) being an implicit parameter. We expect a linear relationship for each site with a slope equal to

$$\frac{dB^a_{0,i}}{dm^a_{\rm U}} = \frac{\mu_0}{v_0}[C^{aa}_i(\mathbf{q}=\mathbf{0}) + \mathfrak{H}^{aa}_i]. \quad (5)$$

Using data from Tables II and V, we compute $dB^a_{0,2b}/dm^a_{\rm U}$ $=45$ mT/μ_B, and $dB^a_{0,4j}/dm^a_{\rm U}=258$ mT/μ_B. In Fig. 11 the two spontaneous fields are displayed versus the uranium magnetic moment at four pressures. Strictly speaking, we should plot the $B^a_{0,i}$ fields versus the localized uranium magnetic moment rather than versus $m^a_{\rm U}$. However, as recalled in Sec. II, the localized uranium magnetic moment has been determined only at ambient pressure and at 1.4 GPa and the difference between the two moments is negligible at ambient pressure.

Although the data points are rather distributed around the expected linear behavior, in particular, for the muon at position 4j, B^a_i scale reasonably well with $m^a_{\rm U}$ up to $m^a_{\rm U}$ $\simeq 1.28\mu_B$. However, the slope is 10% larger than expected for the muon at position 2b and smaller by 28% for the other position. As discussed before, these differences probably reflect the effect of the muon zero-point motion. We have inferred at the end of Appendix B that the spin-orbit interaction of the uranium electrons should be taken into account for the analysis of the Knight shift. It may also have an influence on the value of the slopes.

The observed strong deviation in the SP phase from a simple linear relationship between the spontaneous field at the 4j site and the magnetic moment carried by a uranium atom is one of the key experimental results obtained from this study. A similar deviation could exist for the 2b site but it cannot be established with certainty. A by-product of our studies is the confirmation that the SP phase appears at a constant value of the ordered uranium moment, independent of the applied pressure. The loss of linearity is seen at all the pressures but is observed in a larger range of magnetic moments at ambient pressure.

Let us discuss the results shown in Fig. 11 in terms of the local fields at the two muon sites. According to Eq. (A3), $B^a_{0,4\mathrm{j}}$ is proportional to the sum of two terms of opposite sign with $C^{aa}_{4\mathrm{j}}(\mathbf{q}=\mathbf{0})>0$ (see Table II) and $\mathfrak{H}^{b\perp}_{4\mathrm{j}}<0$ (see Table V). In addition, $|C^{aa}_{4\mathrm{j}}(\mathbf{q}=\mathbf{0})|>|\mathfrak{H}^{b\perp}_{4\mathrm{j}}|$. $C^{aa}_{4\mathrm{j}}(\mathbf{q}=\mathbf{0})$ is not expected to depend significantly on which of the ferromagnetic phase is investigated: it is a fixed parameter. Hence, the detected increase in $B^a_{0,4\mathrm{j}}$ is the signature of a shrinking of $\mathfrak{H}^{b\perp}_{4\mathrm{j}}$ in the SP phase relative to the WP phase. Larger is m^a_{U}, stronger is the reduction in the hyperfine constant. The variation is nonlinear. That this effect is only clearly seen at the 4j site is not surprising, giving the extremely small value of $\mathfrak{H}^{b\perp}_{2\mathrm{b}}$, at least at ambient pressure. A shrinking of $\mathfrak{H}^{b\perp}_{4\mathrm{j}}$ versus pressure has also been inferred above following the interpretation of the data of Fig. 9. This latter effect is not clearly seen in the data of Fig. 11. Therefore, it must be negligible in comparison to the shrinking of $\mathfrak{H}^{b\perp}_{4\mathrm{j}}$ in the SP phase.

Referring to the discussion of the origin of the hyperfine interaction given in Appendix A 1, we attribute the shrinking of $\mathfrak{H}^{b\perp}_{4\mathrm{j}}$ in the SP phase relative to the WP phase to a decrease in the product of the electronic density at the Fermi level by the volume enclosed by the Fermi surface. This electronic effect is clearly observed up to 0.85(2) GPa. Our experimental precision does not allow us to decide whether it is still present at 1.00(2) GPa.

As recalled in Sec. II, an increase in the carrier concentration below T_X has been inferred from Hall-coefficient measurements.[23] Taking the reasonable assumption that the carriers are the electrons, the volume encapsulated by the Fermi surface is deduced to be larger below T_X. Combined with the inferred shrinking of $\mathfrak{H}^{b\perp}_{4\mathrm{j}}$, we deduce that the electronic density in the SP phase is strongly reduced compared to the same density in the WP phase.

2. High-pressure results

In Fig. 12 the two spontaneous fields and the initial sample asymmetry measured at 1.33(2) GPa are displayed versus temperature. In contrast to their thermal behavior at low pressure, the fields abruptly vanish at $T_{\mathrm{C}}\simeq 19.5$ K, confirming the first-order nature of the magnetic phase transition under 1.33(2) GPa. Looking at the temperature dependence of the sample asymmetry, $a_{2\mathrm{b}}+a_{4\mathrm{j}}$, we note it is constant with the expected value up to 16 K and then drops rather sharply at 18 K. Since the sample asymmetry is a measure of the magnetic volume, see the discussion at the beginning of Sec. IV B, we infer that there is no real phase separation: 100% of the volume is magnetic.

C. Spin-lattice relaxation rate

Since in this section we shall discuss spectra recorded with the longitudinal field geometry, it is the asymmetry $a_0 P^{\mathrm{exp}}_Z(t)$ which is measured. Because we shall only report on measurements in the paramagnetic phases and in the ferromagnetic phases with the experimental geometry such that the two spontaneous fields at the muon sites are parallel to **Z**, we expect a simple relaxing signal from the sample. Assuming the relaxation function for each site to be well modeled by an exponential function characterized by a relaxation rate with an extremely small value, the relaxation arising from the two muon sites should be described by a single exponential relaxation function characterized by the relaxation rate λ_Z. In fact this model is supported by the measured spectra. We write

$$a_0 P^{\mathrm{exp}}_Z(t) = a_{\mathrm{s}} \exp(-\lambda_Z t) \tag{6}$$

for spectra recorded without the pressure cell and

$$a_0 P^{\mathrm{exp}}_Z(t) = a_{\mathrm{s}} \exp(-\lambda_Z t) + a_{\mathrm{KT}} P_{\mathrm{KT}}(t) \tag{7}$$

for measurements with the sample in the pressure cell.

The spectra were taken at ambient pressure and at 0.95(2) GPa. For both cases, as shown in Sec. IV A, the magnetic phase transition from the PM to the WP is second order. This is an important point because the theory which will be used to interpret the relaxation data, and summarized in Appendix A, requires the magnetic phase transition to be second order. A zero-field spectrum taken at ambient pressure (and outside the pressure cell) in the SP phase is illustrated in Fig. 19. A zero-field spectrum recorded at 0.95(2) GPa in the critical regime is displayed in Fig. 4.

Figure 13 displays $\lambda_Z(T)$ in the critical regime at ambient pressure and 0.95(2) GPa measured for $\mathbf{S}_\mu \perp \mathbf{a}$. With the

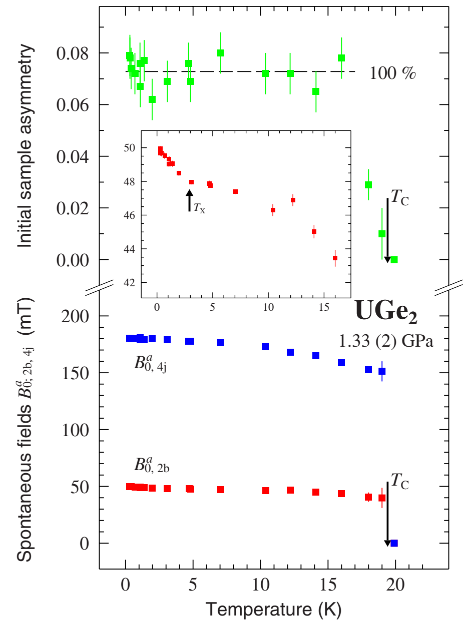

FIG. 12. (Color online) The initial sample asymmetry and the two spontaneous magnetic fields measured for UGe_2 at 1.33(2) GPa versus the temperature. The value of T_{C} deduced from these data is marked by arrows. The insert displays the thermal dependence of $B^a_{0,2\mathrm{b}}$ at low temperature. It serves to determine T_X. These measurements were performed with a cylinder cut from crystal A. That crystal was annealed as explained in Sec. III.

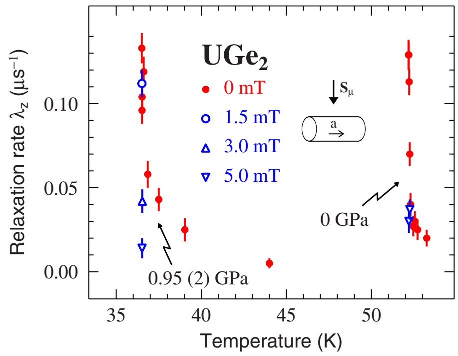

FIG. 13. (Color online) An overview of the results from our study of the paramagnetic critical spin dynamics for $\mathbf{S}_\mu \perp \mathbf{a}$ at the GPD spectrometer. The sample was a cylinder cut from sample A placed in the pressure cell. The temperature T_C was defined as the temperature at which the spontaneous fields, which appear below T_C, disappear. At ambient pressure T_C=52.16(1) K is obtained and T_C=36.48(1) K at 0.95(2) GPa. The spin dynamics as probed by the measurements of λ_Z are remarkably similar at the two pressures.

sample available we could not investigate the spin dynamics for $\mathbf{S}_\mu \| \mathbf{a}$ under pressure. The data present two remarkable features. The spin dynamics probed at the two pressures are quite similar and the relaxation rates are quenched for very small longitudinal magnetic fields. A mere 5 mT is enough to suppress most of the relaxation.

For the analysis of λ_Z it is of interest to draw it versus the reduced temperature scale $\tau=(T-T_C)/T_C$. This is done in Fig. 14 for the zero-field data plotted in Fig. 13.

An inspection of the results shown in Fig. 14 and in Ref. 4 confirms the similarity of the data at ambient pressure. A saturation of λ_Z close to T_C is observed for all the cases. Strictly speaking the two sets of data recorded at ambient pressure for $\mathbf{S}_\mu \perp \mathbf{a}$ should be equivalent. This is not quite so. Two quantitative differences appear: λ_Z is larger in Fig. 14 at low τ and the extension of the plateau at low τ is smaller. Two sets of data have been recorded at different spectrometers using different types of muon beams (pulsed and quasicontinuous). In addition, two different samples were used. Whereas the data of Ref. 4 were obtained from an as-grown single crystal (crystal B), the spectra used to deduce λ_Z displayed in Fig. 13 (and therefore in Fig. 14) were recorded

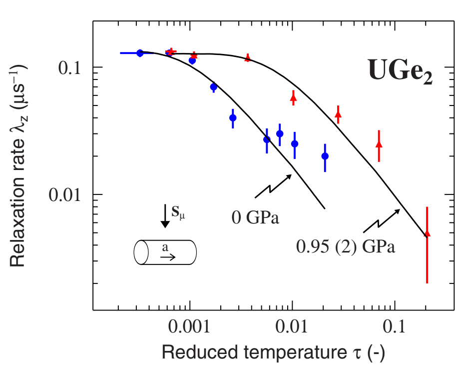

FIG. 14. (Color online) λ_Z versus the reduced temperature $\tau=(T-T_C)/T_C$ for the zero-field data presented in Fig. 13. The solid lines are the results from fits to a model discussed in the main text.

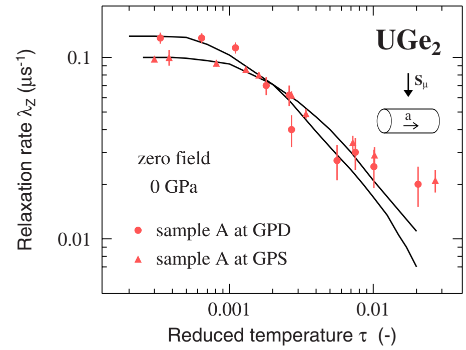

FIG. 15. (Color online) Comparing the results from sample A obtained at two different spectrometers. We present λ_Z versus reduced temperature $\tau=(T-T_C)/T_C$ recorded at the GPD and GPS spectrometers. The solid lines are the results from fits to a model discussed in the main text. We recall that this model describes the critical spin dynamics and is therefore not expected to model the data outside the critical regime.

with a sample cut from an annealed crystal (crystal A). The measured difference in $\lambda_Z(T)$ could result from improper modeling of the background or from sample quality differences or both of them. In order to determine its origin a series of measurements were done at GPS. The comparison of the results for sample A obtained at GPS and GPD allows us to test the validity of the background used to model the contribution of the pressure cell to the measured asymmetry. Comparing the published results[4] and the GPS data allows us to gauge the influence of the sample quality (A versus B crystals). A complete analysis shows that measuring the same sample A at different instruments yields slightly different results; see Fig. 15. But the observed difference between the already published data and the ones of Fig. 13 is mainly due to the fact that samples A and B are really different.

A complete discussion is given elsewhere.[42] The former sample is probably of better quality as reflected by the fact that its maximum in $\lambda_Z(T)$ is more intense. We recall that the longitudinal-field spectra recorded for sample B were analyzed with a model which suggests that defects were present.[4] On the other hand, a simple exponential function provides a proper account of a spectrum recorded under a small longitudinal field for sample A. In the following we shall mostly discuss the experimental data recorded for that sample.

In spite of the sample and instrument dependencies of the results on the critical spin dynamics in UGe_2, the comparison between ambient pressure and a pressure of 0.95(2) GPa should be considered reliable since here it concerns a single experiment on the same sample at same spectrometer for different pressures.

Far outside T_C there is the possibility that the muon relaxation is driven by the nuclear magnetic moments of the ^{73}Ge isotope. Since the relaxation function is exponential, we are in the motional narrowing limit. The narrowing of the field distribution at the two muon sites would then arise from the muon diffusion rather than the nuclear spins. An investigation of the field dependence well below T_C follows the predicted behavior given at Eq. (A12). It allows us to deduce $\nu_f \simeq 1\ \mu s^{-1}$. Since we compute $\Delta=0.02\ \mu s^{-1}$ for the nuclear

TABLE I. Comparison of the directly measured parameters $q_D\xi_0^+$ or $q_D\xi_0^-$, $\mathcal{W}a_L$, $\mathcal{W}a_T$, and ν_f and inferred parameters a_L/a_T, m_{cond}, q_D, ξ_0^+, or ξ_0^- for samples extracted from crystal A under different experimental conditions. The measurements have been done at the GPS and GPD spectrometers.

Geometry	$\mathbf{S}_\mu \parallel \mathbf{a}$		$\mathbf{S}_\mu \perp \mathbf{a}$		
Spectrometer	GPS	GPS	GPS	GPD	GPD
Pressure	0 GPa	0 GPa	0 GPa	0 GPa	0.95(2) GPa
Temp. range	$T>T_C$	$T<T_C$	$T>T_C$	$T>T_C$	$T>T_C$
$q_D\xi_0^+$ or $q_D\xi_0^-$	0.0065(6)	0.0071(7)	0.0080(4)	0.0052(7)	0.0182(5)
$\mathcal{W}a_L$ (μs^{-1})	0.27(3)	0.24(2)	0.56(2)	0.82(2)	0.72(1)
$\mathcal{W}a_T$ (μs^{-1})	0.010	0.015	0.015	0.010	0.027
a_L/a_T	27	16	37	82	26.7
ν_f (μs^{-1})	~2.8(4)	~2.8(4)	~2.8(4)	2.8(4)	1.5(3)
m_{cond} (μ_B)	0.025(2)	0.027(2)	0.018(1)	0.015(1)	0.011(1)
q_D (Å^{-1})	0.0035(2)	0.0033(2)	0.0044(4)	0.0050(2)	0.0044(2)
ξ_0^+ or ξ_0^- (Å)	2.2(2)	2.2(3)	1.6(2)	1.1(2)	4.3(4)

magnetic field, the muon diffusion mechanism predicts $\lambda_Z = 10^{-3}\ \mu s^{-1}$. This is ten times smaller than measured. This means that an other mechanism than the muon diffusion drives the muon relaxation. Deep in the paramagnetic state the fluctuations of the full uranium magnetic moments cannot account for the observed relaxation since Δ would be expected to be far larger than measured. The relaxation mechanism in the paramagnetic and ordered states is unclear. More experimental data are required.

However, the most exciting experimental results obtained from the spin-lattice relaxation measurements is the temperature and field behavior of λ_Z close to T_C. The zero-field thermal critical behaviors of λ_Z have been fitted to Eq. (A13). The fits for the GPD data are shown in Figs. 14 and 15. An example for GPS data is illustrated in Fig. 15. The extracted experimental parameters, the products $q_D\xi_0^+$, $q_D\xi_0^-$, $\mathcal{W}a_L$, and $\mathcal{W}a_T$, are summarized in Table I.

We recall that the cylinder available at GPD allowed us to probe only the spin dynamics for the initial muon beam polarization perpendicular to **a**. A comment on the uncertainties for the data of the table is in order. The value of $\mathcal{W}a_T$ was fixed to an appropriate value during a fitting procedure because due to its small value it was difficult to obtain a precise value. Error bars are therefore not given for $\mathcal{W}a_T$ neither for the ratio a_L/a_T. The difficulty in the determination of a_T is at the origin of the relatively disperse values for this ratio.

As already mentioned, there is a dependence on spectrometers: compare the results for the measurements at GPS and GPD at ambient pressure for $\mathbf{S} \perp \mathbf{a}$. But still, the measured parameters are in reasonable agreement. In general, $\mathcal{W}a_T$ is much smaller than $\mathcal{W}a_L$.

In addition to the zero-field measurements, small longitudinal fields have been applied at fixed temperature, see Fig. 13. At a given temperature, combining the result from the zero-field measurement which determines $\lambda_Z(0)$ and the measurements of $\lambda_Z(B_{ext})$, an estimate of the fluctuation rate ν_f can be made using Eq. (A12). The experiments in magnetic field have not been performed in all cases. If not, then a value of ν_f is estimated by assuming the same value as for the case that the sample was measured in a magnetic field. The estimation is indicated by the symbol ~. Before analyzing the data further, their three main features in the vicinity of T_C will be first summarized.

We recall that the magnetic anisotropy of UGe_2 is known to be large; see Sec. II. This is confirmed by the μSR Knight shift measurements as illustrated in the Clogston-Jaccarino plots presented in Fig. 18. A magnetic field parallel to **a** induces a large shift whereas a field perpendicular to **a** induces a very small shift. However, as shown in Ref. 4 the dependence of the relaxation rate $\lambda_Z(T)$ on the orientation of $\mathbf{S}_\mu$ with respect to **a** shows very weak anisotropy. μSR is generally very sensitive to the anisotropy of the magnetic fluctuations as was nicely demonstrated for the intermetallics $NdRh_2Si_2$.[43]

The second remarkable property of the measured critical spin dynamics is its extreme sensitivity to an applied magnetic field. The relaxation rate is suppressed by a magnetic field on the order of 2–5 mT. Susceptibility data shows that a magnetic field of 5 mT induces a magnetic moment of less than $0.01\mu_B/U$. Therefore it is hard to imagine that the fluctuations of the full U moments, which have a saturation magnetization of $1.4\mu_B/U$ at low temperatures, are suppressed by a field of 5 mT. Moreover, we have measured a correlation time of $\approx 0.4\ \mu s$. This can be considered to be quasistatic and does not reflect the expected strong dynamics for the large magnetic moment on the U atoms. Since according to Eq. (A12) the value of λ_Z in zero field is given by $\lambda_Z = 2\Delta^2/\nu_f$, it follows that $\Delta/\gamma_\mu \approx 0.3$ mT. This indicates a very small distribution in local magnetic fields at the muon site. It cannot arise from the full U moments.

The third remarkable feature is the thermal behavior of λ_Z which is not unlike the one found for the metallic ferromagnets Fe, Ni, Gd, and $GdNi_5$ at ambient pressure:[44–46] the relaxation rate is found to saturate when approaching T_C.

Based on these observations it is proposed that the muon spin is relaxed by the magnetic moments of the conduction electrons. It is expected that the magnetic anisotropy of these electrons is much smaller than the one of the localized magnetic moments. Because of the strong electronic correlations in UGe_2 reflected, for example, by the large Sommerfeld coefficient (see Sec. II), their magnetic fluctuations are slow. Moreover, this assumption can account for the observed small Δ value.

So far only values for the products $\mathcal{W}a_{\rm L}$ and $\mathcal{W}a_{\rm T}$ were presented. In order to compute $\mathcal{W}$ appearing in Eq. (A14), estimates for $a_{\rm L}$ and $a_{\rm T}$ should be made. Two muon sites have been found and taking the weighted averages, we have $a_{\rm L}=0.55a_{\rm L,2b}+0.45a_{\rm L,4j}$ and $a_{\rm T}=0.55a_{\rm T,2b}+0.45a_{\rm T,4j}$. It has been established theoretically that $a_{{\rm L},i}$ and $a_{{\rm T},i}$ depend generally on the dipole and hyperfine tensors. However, we have inferred above that only the conduction-electron magnetic moments contribute to the relaxation. Therefore, it seems reasonable in the case of UGe_2 that only the two hyperfine tensors matter for determining the parameters $a_{{\rm L},i}$ and $a_{{\rm T},i}$. Let us first consider the site at position 2b for which the hyperfine tensor is scalar to a good approximation. From Table V we get $\mathfrak{H}_{2b}^{b^\perp}=\mathfrak{H}_{2b}^{b^\parallel}=\mathfrak{H}_{2b}=-0.025$. Since $a_{\rm L,2b}=(1-\mathfrak{H}_{2b})^2$ and $a_{\rm T,2b}=2\mathfrak{H}_{2b}^2$,[44] we compute $a_{\rm L,2b}=1.05$ and $a_{\rm T,2b}=0.001$. For the muon at position 4j the hyperfine tensor is not completely determined. For definitiveness we assume that tensor to be scalar and using the data of Table IV, we get $a_{\rm L,4j}=0.62$ and $a_{\rm T,4j}=0.089$. Therefore we compute $a_{\rm L}=0.85$ and $a_{\rm T}=0.04$ with a ratio $a_{\rm L}/a_{\rm T}=21$, which is close to the values given in Table I, considering the uncertainty in the determination of the weight of the transverse fluctuations.

Our discussion has shown that it is the magnetic moments of the conduction electrons which are at the origin of the measured relaxation. Therefore we identify μ in Eq. (A14) with $m_{\rm cond}$. Hence, now we can estimate values for $m_{\rm cond}$, the dipolar wave vector $q_{\rm D}$ and the correlation lengths ξ_0^+ and ξ_0^-. They are given in Table I. Clearly, in spite of the instrument dependence, the magnitude of $m_{\rm cond}$ is $0.015(5)\mu_{\rm B}$ at ambient pressure and at 0.95(2) GPa, taking into account the instrument dependence of our estimate. The value at ambient pressure measured here is consistent with the one extracted from the analysis of the neutron-diffraction data (see Sec. II). A comparison cannot be done for the 0.95(2) GPa result since there is no neutron data available. Within the experimental uncertainty, $q_{\rm D}$ is independent of the pressure intensity. The main difference, leading to different critical dynamics at high pressure relative to ambient pressure (see Fig. 14), is the enhancement of the correlation length ξ_0^+ for the magnetic fluctuations in the paramagnetic state. However, the correlation lengths ξ_0^+ and ξ_0^- are always found to be on the order of the distance between uranium atoms. This is in contrast to expectation if we refer to d transition metals close to ferromagnetic instabilities. For these weak ferromagnets characterized by itinerant magnetic electrons with small magnetic moments, the lengths are an order of magnitude larger.[47] The short correlation lengths found in UGe_2 mean that the width of the quasielastic peak resulting from magnetic fluctuations, which may be measured by neutron scattering, should be proportional to the wave vector of these fluctuations. This is effectively observed for the antiferromagnet UPt_3 (Ref. 48) for which the uranium magnetic moment is extremely small. A qualitative understanding of the neutron data is reached for UPt_3 recognizing that the spin-orbit coupling in a uranium compound cannot be neglected. This discussion suggests direction for theoretical and further experimental works aimed at understanding the measured slow spin dynamics in UGe_2.

V. SUMMARY AND COMPARISON WITH OTHER ACTINIDE SYSTEMS

We shall first summarize the magnetic and electronic properties of UGe_2 derived from this study. We have detected signatures of T_X which is the temperature at which the compound changes from the WP phase to the SP phase. Interestingly, T_X at 1.00(2) GPa and below does not correspond to a crossover but to a thermodynamic phase transition. This is inline with the result of the specific heat study of Tateiwa and collaborators who established the thermodynamic nature of the transition at T_X for pressure slightly below p_c^* ($p_c^* \simeq 1.2$ GPa).[13] Compared to previous works, we have found that this temperature is still defined at 1.33(2) GPa. Therefore we have evidenced that T_X does not vanish at p_c^*, as often suggested. Referring to Fig. 2 it must be noted that the temperature scale for $T_{\rm s}$ is multiplied by a factor 5 unlike that of T_X. An extrapolation of T_X to pressures higher than 1.33 GPa suggests in fact that T_X vanishes at p_c. Of course more data points would be needed for 1.2 GPa$<p<p_c$ to definitively confirm it. The signature that we have for T_X at 1.33(2) GPa is different from that we have at 1.00(2) GPa and below. In both cases, the average field at the muon presents an anomaly, but only at 1.00(2) GPa and below, the field fluctuations do show a maximum. Therefore the order of the transition might have changed. Since T_X is not identified by magnetization measurements for $p \gtrsim 1.2$ GPa, our result indicates that the origin of the transition could be related to conduction electrons. Interestingly, the signature of T_X is only observed for muons located in the 2b site at 1.33(2) GPa while it is more directly seen for muons located in the 4j site at lower pressures.

Another key information from the present study is the homogeneity of the compound at 1.33(2) GPa, i.e., there is no spontaneous magnetic phase separation as it enters its magnetically ordered state. A clear difference between the WP and SP phases has been found, at least up to 0.85(2) GPa. The hyperfine constant is much smaller in the low-temperature phase, that is, in the strongly polarized phase. Combined with results from Hall-coefficient measurements at ambient pressure, we infer that the density of states at the Fermi surface shrinks as the compound is cooled down through T_X, at least up to 0.85(2) GPa.

The present study of the critical spin dynamics confirms the preliminary result some of us published in 2002: UGe_2 has to be viewed schematically as a two subsets electronic system.[4] The localized $5f$ electrons are at the origin of most of the uranium magnetic density. The itinerant electrons carry a small magnetic moment which is relatively isotropic. The previous study was performed at ambient pressure on a sample which was not annealed. Here we have investigated an annealed sample at ambient pressure and at 0.95(2) GPa, a temperature at which the paramagnetic-ferromagnetic transition is still second order, a property required to derive physical information from the measurements. In addition, sample B was reinvestigated at ambient pressure at the GPS spectrometer. The responses from the annealed and unannealed samples are qualitatively the same. The critical spin dynamics observed for UGe_2 by μSR measurements stems from itinerant electrons characterized by a small magnetic moment. We do not detect the signature of the localized $5f$ electrons. This may be due to a strong motional narrowing of the μSR signal for these electrons. The last discovered ferromagnetic superconductor, UCoGe, exhibits a uranium magnetic moment of only $0.07\mu_b$ at saturation.[49] Interestingly, this is in the range of the value for the moment deduced here for the conduction electrons in UGe_2. A finite λ_Z is only detected in the ferromagnetic state.[49] We now consider UGe_2 in relation to other actinide compounds.

The small value of the ratio $m_{\mathrm{cond}}/m_{\mathrm{U}}^{a}$ supports the picture that the bulk magnetic properties of UGe_2 derive from nearly localized f electrons. The superconductor $PuCoGa_5$ is also a compound for which such a picture is put forward.[50] Obviously, the dominant localized character of the $5f$ electrons in a metallic compound is not a generality. The ferromagnetic cubic fcc Laves UFe_2 offers a counter example for which a strong itinerant $5f$ character has been nicely shown by neutron form-factor measurements.[51] The dual nature of the $5f$ electrons has been theoretically suggested to result from the interplay of intra-atomic correlations as described by Hund's rules and a weakly anisotropic hopping (hybridization); see Ref. 52 and references therein.

VI. POSSIBLE FUTURES μSR MEASUREMENTS ON UGe_2

The purpose of this study has been to determine from μSR techniques physical properties of the ferromagnetic superconductor UGe_2. We have obtained information on the magnetic and electronic properties of the compound. Combining these properties with the ones listed in Appendix B, we could attempt to discuss the origin of the superconductivity of UGe_2 and compared with available theoretical models. We shall refrain from doing it, simply because we believe more experimental information is needed for a meaningful comparison with theoretical models. We prefer to suggest two series of μSR experiments which would help to better pinpoint the physics of the compound. They are technically demanding.

It would be quite interesting to study $\lambda_{X,i}$ and $B_{0,i}^{\mathrm{a}}$ above 1.0 GPa around T_X to determine whether the peaks in $\lambda_{X,i}$ we observe at 1.00(2) GPa (see Fig. 8) are still present at higher pressure and if T_X as probed by $B_{0,i}^{\mathrm{a}}(T)$ effectively vanishes at p_c. This would yield information on the nature of the transition between the WP and SP phases and its possible relation to superconductivity. Related to this physics, a study of λ_Z at and above 1.0 GPa around T_X has to be done. These two types of measurements give the possibility to derive information on the spin dynamics of the compound. This is crucial if the Cooper pairing is due to magnetic fluctuations.

It would be useful to carry out zero-field measurements at low temperature under a pressure of ~1.25 GPa to determine whether a spontaneous flux line lattice exists. We note that a signature of the lattice has been found recently for UCoGe.[49] Performing the measurements at extremely low temperature (0.1 K, for example) gives two advantages. First, lower is the temperature, smaller is the magnetic penetration depth. This means that the standard deviation of the FLL field distribution is larger. The FLL is more easily detected. Second, since the upper critical field increases as the sample is cooled down, the cutoff due to the vortex core[53] is expected to be attenuated at low temperature.

ACKNOWLEDGMENTS

We thank A. de Visser for his interest in this work and useful discussions. Part of this work was performed at the Swiss Muon Source (Paul Scherrer Institute, Villigen, Switzerland). This research project has been partially supported by the European Commission under the 6th Framework Programme through the Key Action: Strengthening the European Research Area, Research Infrastructures (Contract No. RII3-CT-2003-505925). Three of us (A.Y., P.D.R., and A.A.) were partially supported by the "Programme d'action integrée PAI franco-suisse Germaine de Staël."

APPENDIX A: μSR THEORETICAL BACKGROUND

In this appendix we summarize the information required for understanding the discussion given in the main text on the magnetic field at the muon sites and the spin-lattice relaxation rate. We refer to Refs. 33, 34, and 54 for more information.

1. Magnetic field at the muon site

We denote as $\mathbf{B}_{\mathrm{ext}}$ the external applied field, $\mathbf{B}_0$ as the spontaneous field at the muon site, $\mathbf{B}'_{\mathrm{dip}}$ as the dipole field inside the Lorentz sphere, $\mathbf{B}_{\mathrm{Lor}}$ as the Lorentz field, and $\mathbf{B}_{\mathrm{hyp}}$ as the hyperfine field. We have the relation

$$\mathbf{B}'_{\mathrm{dip}} + \mathbf{B}_{\mathrm{Lor}} = \frac{\mu_0}{v_0}\mathbf{C}(\mathbf{q}=\mathbf{0})\mathbf{m}_{\mathrm{U}}, \tag{A1}$$

where $\mathbf{C}(\mathbf{q}=\mathbf{0})$ is a tensor given, for example, in Ref. 44, and v_0 the volume per uranium ion, i.e., $v_0=abc/4=62.00$ Å^3 in the case of UGe_2. The symmetric tensor $\mathbf{C}(\mathbf{q})$ is evaluated at the Brillouin-zone center, i.e., $\mathbf{q}=\mathbf{0}$, and the trace of $\mathbf{C}(\mathbf{q}=\mathbf{0})$ is equal to one. Several interstitial positions with a high symmetry are available in UGe_2. These are the best candidates for muon stopping sites. Table II contains the value of the elements of $\mathbf{C}(\mathbf{q}=\mathbf{0})$ for several candidate muon sites.

With the reasonable hypotheses that the hyperfine interaction is short range and diagonal in the reference frame adapted to the crystal symmetry of UGe_2 (the reference frame $\{a,b,c\}$), we have

$$B_{\mathrm{hyp}}^{\alpha} = \frac{\mu_0}{v_0}\mathfrak{H}^{\alpha\alpha} m_{\mathrm{U}}^{\alpha}, \tag{A2}$$

where $\mathfrak{H}^{\alpha\alpha}$ is an hyperfine tensor element.[44] In this paper, we use the notations $\{\alpha,\beta\}=\{a,b,c\}$. The hyperfine interaction results from the indirect Ruderman-Kittel-Kasuya-Yosida interaction between the muon spin and the uranium magnetic moments. It contains valuable information on the exchange interaction between the $5f$ electrons and the conduction electrons, the Fermi-contact interaction between the muon spin

TABLE II. Calculated elements of the tensor $\mathbf{C}(\mathbf{q}=\mathbf{0})$ at several candidate stopping sites for the muon in UGe_2. We use the Wyckoff notation to label the sites and give their reduced coordinates. The tensor components are given relative to axes parallel to the orthorhombic crystallographic axes, i.e., $\{a,b,c\}$. For the 4i and 4j muon sites, two uranium atoms and two germanium atoms form a tetrahedron in which the muon is located. For the 4i site, we assume the muon to be at the center of the tetrahedron. The value of the tensor elements is only slightly dependent on the free reduced coordinate y. On the other hand, as shown in the table, the tensor elements are strongly y dependent for site 4j. The position with $y=0.1740$ corresponds to the muon at the center of the tetrahedron. For $y=0.1916$ the muon is right in the middle between the two germanium atoms of the tetrahedron and for $y=0.1415$ in the middle of the axis through the two uranium atoms.

Site	Coupling tensor $\mathbf{C}(\mathbf{q}=\mathbf{0})$
2b $(0,\frac{1}{2},0)$	$\begin{pmatrix} 0.264 & 0 & 0 \\ 0 & 0.442 & 0 \\ 0 & 0 & 0.294 \end{pmatrix}$
2d $(\frac{1}{2},\frac{1}{2},\frac{1}{2})$	$\begin{pmatrix} -0.672 & 0 & 0 \\ 0 & 2.369 & 0 \\ 0 & 0 & -0.697 \end{pmatrix}$
4e $(\frac{1}{4},\frac{1}{4},0)$	$\begin{pmatrix} 0.023 & \pm 0.336 & 0 \\ \pm 0.336 & 0.173 & 0 \\ 0 & 0 & 0.804 \end{pmatrix}$
4f $(\frac{1}{4},\frac{1}{4},\frac{1}{2})$	$\begin{pmatrix} 0.328 & \pm 1.663 & 0 \\ \pm 1.663 & 1.748 & 0 \\ 0 & 0 & -1.076 \end{pmatrix}$
4i (0,0.1590,0)	$\begin{pmatrix} -0.672 & 0 & 0 \\ 0 & -0.680 & 0 \\ 0 & 0 & 2.352 \end{pmatrix}$
4j $(\frac{1}{2},0.1916,\frac{1}{2})$	$\begin{pmatrix} 1.594 & 0 & 0 \\ 0 & 0.207 & 0 \\ 0 & 0 & -0.801 \end{pmatrix}$
4j $(\frac{1}{2},0.1740,\frac{1}{2})$	$\begin{pmatrix} 2.066 & 0 & 0 \\ 0 & -0.228 & 0 \\ 0 & 0 & -0.838 \end{pmatrix}$
4j $(\frac{1}{2},0.1415,\frac{1}{2})$	$\begin{pmatrix} 2.508 & 0 & 0 \\ 0 & -0.641 & 0 \\ 0 & 0 & -0.867 \end{pmatrix}$

and the conduction-electron spin, and the conduction-electron susceptibility, see, e.g., Ref. 55. In fact, the hyperfine constant is found proportional to the product of the electronic density at the Fermi level by the volume enclosed by the Fermi surface. However, it also depends on the spin-density enhancement factor, reflecting the muon-induced changes in the local electronic structure. This factor is difficult to estimate.[34] While the effective exchange and Fermi-contact interactions have a strong atomic character, and therefore should not depend drastically on the experimental conditions, such as the temperature and the pressure, we expect the electronic susceptibility and the Fermi volume, and therefore $\mathfrak{H}^{\alpha\alpha}$, to be sensitive to the experimental conditions.

Since $\mathbf{B}_0$ is found parallel to the easy $\mathbf{a}$ axis

$$B_0^a = \frac{\mu_0}{v_0}[C^{aa}(\mathbf{q}=\mathbf{0}) + \mathfrak{H}^{aa}]m_{\mathrm{U}}^a. \tag{A3}$$

The measured frequency shift is defined by the relation

$$K_{\mathrm{exp}} = \frac{\nu - \nu_{\mathrm{ext}}}{\nu_{\mathrm{ext}}}. \tag{A4}$$

Here ν is the measured frequency and we have introduced the notation $\nu_{\mathrm{ext}}=(\gamma_\mu B_{\mathrm{ext}})/(2\pi)$.

We assume the susceptibility tensor to be diagonal in the reference frame $\{a,b,c\}$ with elements χ^a, χ^b, and χ^c. We suppose $\mathbf{B}_{\mathrm{ext}}$ to be applied along the α axis. We can write

$$K_{\mathrm{exp}}^\alpha = \mathcal{F}^{\alpha\alpha}\chi^\alpha + K_{\mathrm{cond}} \tag{A5}$$

with the definition

$$\mathcal{F}^{\alpha\beta} = C^{\alpha\beta}(\mathbf{q}=\mathbf{0}) + \left(-\frac{1}{3} + \mathfrak{H}^{\beta\beta}\right)\delta^{\alpha\beta}. \tag{A6}$$

The last term in Eq. (A5) phenomenologically accounts for the approximately isotropic contribution of the conduction electrons to the Knight shift. We write $K_{\mathrm{cond}}=A_{\mathrm{cond}}\chi_{\mathrm{cond}}$, where A_{cond} is an hyperfine constant and χ_{cond} the conduction-electron susceptibility which is temperature independent. We note the relation

$$\sum_\alpha \mathcal{F}^{\alpha\alpha} = \sum_\alpha \mathfrak{H}^{\alpha\alpha}. \tag{A7}$$

It is interesting to consider the angle dependence of the Knight shift. According to Schenck[56]

$$K_{\mathrm{exp}}(\theta) = K_{\mathrm{exp},0} + \Delta K_{\mathrm{exp}}\cos^2\theta \tag{A8}$$

with

$$K_{\mathrm{exp},0} = \mathcal{F}^{xx}\chi^x, \quad \Delta K_{\mathrm{exp}} = \mathcal{F}^{zz}\chi^z - \mathcal{F}^{xx}\chi^x. \tag{A9}$$

The angle θ is the polar angle of $\mathbf{Z}$ in $\{x,y,z\}$ which is the reference frame adapted to the symmetry of the compound. We have recorded spectra with the rotating axis parallel either to the $\mathbf{b}$ or $\mathbf{c}$ axes of the crystal. For the former case we can identify the $\mathbf{x}$, $\mathbf{y}$, and $\mathbf{z}$ axes with the $\mathbf{a}$, $\mathbf{b}$, and $\mathbf{c}$, respectively, and in the latter case with the $\mathbf{b}$, $\mathbf{c}$, and $\mathbf{a}$ axes, respectively. The previous equation is valid if $C^{ba}(\mathbf{q}=\mathbf{0})=C^{ca}(\mathbf{q}=\mathbf{0})=C^{ab}(\mathbf{q}=\mathbf{0})=C^{ac}(\mathbf{q}=\mathbf{0})=0$, since the hyperfine tensor is assumed to be diagonal in $\{a,b,c\}$. From the measurements of ν_0 and $\Delta\nu$ one expects to be able to estimate two coupling constants using measured values of two susceptibilities. Equation (A8) implies the following frequency relation:

$$\nu(\theta) = \nu_0 + \Delta\nu \cos^2 \theta, \qquad \text{(A10)}$$

where, from the definition written in Eq. (A4)

$$\nu_0 = \nu_{\text{ext}}(1 + \mathcal{F}^{xx}\chi^x),$$

$$\Delta\nu = \nu_{\text{ext}}(\mathcal{F}^{zz}\chi^z - \mathcal{F}^{xx}\chi^x). \qquad \text{(A11)}$$

From the measurements of ν_0 and $\Delta\nu$ one expects to be able to estimate two coupling constants using measured values of two susceptibilities.

2. Spin dynamics probed by μSR

In the simple case of a compound under an external longitudinal field and if only a single mode drives the measured spin dynamics, the spin-lattice relaxation rate λ_Z has the form predicted by Redfield

$$\lambda_Z(B_{\text{ext}}) = \frac{2\Delta^2\nu_{\text{f}}}{\gamma_\mu^2 B_{\text{ext}}^2 + \nu_{\text{f}}^2}, \qquad \text{(A12)}$$

where ν_{f} is the fluctuation rate of the mode and Δ^2/γ_μ^2 the variance of the field distribution at the muon site. Here we neglect any Knight shift.

The theory of critical phenomena for a dipolar Heisenberg ferromagnet used to explain the behavior of λ_Z in the vicinity of T_{C} has been developed by Yaouanc *et al.*[44] It predicts

$$\lambda_Z = \mathcal{W}[a_{\text{L}}I^L(\phi) + a_{\text{T}}I^T(\phi)]. \qquad \text{(A13)}$$

Here L and T refer to the orientation (longitudinal or transverse) of the fluctuation modes relative to their wave vectors $\mathbf{q}$. $\mathcal{W}$ is a nonuniversal constant and $I^{L,T}$ are scaling functions. They account for the longitudinal and transverse fluctuations. The temperature dependence follows through the angle $\phi = \tan^{-1}(q_{\text{D}}\xi)$ where ξ $[\xi = \xi_0(|T - T_{\text{C}}|/T_{\text{C}})^{-\nu}$, where $\nu \simeq 0.69$ and $\xi_0 = \xi(T = T_{\text{C}})]$ is the correlation length and q_{D} is the dipolar wave vector, which determines the relative strength of the dipolar and exchange interactions. Whereas I^L saturates as T approaches T_{C}, I^T displays a divergence. The weighting factors a_{L} and a_{T} depend only on the characteristics of the field at the muon site. The ratio $a_{\text{L}}/a_{\text{T}}$ determines the sensitivity of λ_Z to longitudinal or transverse modes: if $a_{\text{L}}/a_{\text{T}} \gg 1$ one probes mainly the longitudinal fluctuations and therefore λ_Z is roughly temperature independent near T_{C}. In addition, mostly modes with $q \approx q_{\text{D}}$ contribute to the relaxation.[57] This means that Eq. (A12) provides a reasonable description of the field dependence of λ_Z when the longitudinal fluctuations are overwhelmingly driving the relaxation. Denoting μ as the magnetic moment at its origin, μ and q_{D} can be expressed in terms of the two experimental parameters $\mathcal{W}$ and ν_{f} (Ref. 44):

$$\mu = \left(\frac{2\pi^2\hbar^2\gamma_\mu^2}{3P^2}\frac{\nu_{\text{f}}}{\mathcal{W}}\right)^{1/2},$$

$$q_{\text{D}} = \left(\frac{3\pi^2}{\gamma_\mu^2\mu_0 k_{\text{B}}T_{\text{C}}}\mathcal{W}\nu_{\text{f}}\right)^{1/3} \qquad \text{(A14)}$$

with the constant $P = 5.1326$. Since the temperature dependence of λ_Z gives access to the product $q_{\text{D}}\xi_0$, it is possible to extract the value of the correlation length ξ_0 if q_{D} can be estimated. For $T > T_{\text{C}}$ the symbol ξ_0^+ is used while it is ξ_0^- for $T < T_{\text{C}}$.

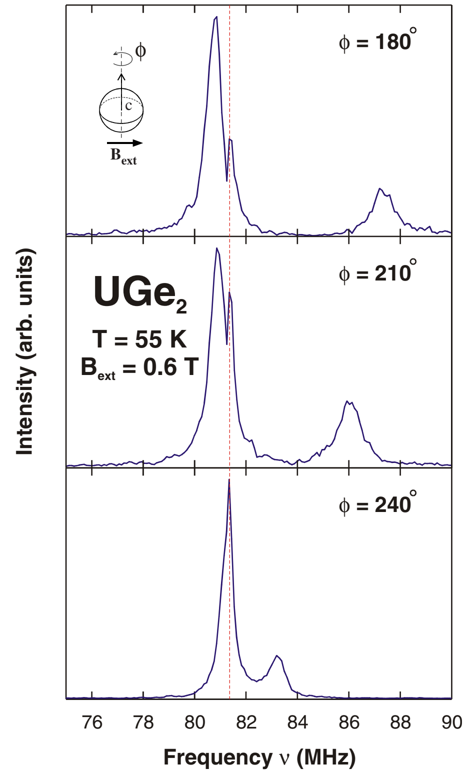

FIG. 16. (Color online) Examples of Fourier transforms of recorded μSR spectra in the paramagnetic state. The angular dependence of the muon frequencies was measured at 55 K by rotating a sphere of single-crystalline UGe_2 around **c** in a field of $B_{\text{ext}} = 0.6$ T perpendicular to the rotation axis. Three frequencies are observed in the Fourier transforms. The signal at $\nu_{\text{BG}} = 81.39$ MHz is indicated by a vertical line. The other two signals come from muons implanted in the sample and show a strong angular dependence. At $\phi = 240°$, the signal of the lower component is mixed with the background signal, i.e., the signal from the sample holder and cryostat wall.

APPENDIX B: THE QUEST FOR THE MUON SITES

In this appendix, using measured Knight shifts in the paramagnetic state and the two spontaneous frequencies at low temperature, both of them recorded at ambient pressure, we determine the two muon localization sites and get information on the hyperfine constants. We start by the presentation of the Knight shifts obtained from the two angular scans performed at the GPS spectrometer. The rotation axis was either the **b** or **c** crystal axis and $B_{\text{ext}} = 0.6$ T. For the choice of the temperature ($T > T_{\text{C}}$), a compromise had to be made between maximization of the Knight shift (closer to T_{C}) and minimization of the spin-spin relaxation rate of the induced muon frequencies (away from T_{C}). A temperature of $T = 55$ K turned out to yield spectra with the best quality. Three Fourier transforms of the spectra recorded during the angular scan around **c** are shown in Fig. 16 as an example.

Three frequencies are clearly seen. The signal at $\nu_{BG} = 81.39$ MHz is indicated by the vertical line. It is attributed to the small fraction of muons stopped in the sample holder and cryostat wall. The two other signals come from muons stopped in the UGe_2 sample and show a strong angular dependence. This points to two magnetically inequivalent muon stopping sites in UGe_2. This is confirmed, as described below, by the detection of two spontaneous frequencies below T_C in zero field.

Since three frequencies are present for all the spectra, the asymmetry $a_0 P_X^{\mathrm{exp}}(t)$ could be analyzed as a sum of three components

$$a_0 P_X^{\mathrm{exp}}(t) = \sum_{i=1}^{3} a_i \exp(-\lambda_{X,i} t)\cos(2\pi\nu_i t - \psi). \qquad \text{(B1)}$$

$\lambda_{X,i}$ is the spin-spin relaxation rate related to frequency ν_i and ψ an angle characterizing the experimental geometry. The asymmetries for the two muon sites in UGe_2 are denoted as a_1 and a_2, and their ratio a_1/a_2 is equal to the ratio of the number of muons stopped at the distinct sites 1 and 2. Although close to the expected value $\nu_{\mathrm{exp}} = 81.32$ MHz, $\nu_3 \equiv \nu_{BG}$ is definitively different. This is attributed to an applied field slightly different from the nominal value of 0.6 T. $\nu_{BG} = 81.39$ MHz corresponds to a field of 0.6005 T.

The three measured muon frequencies are shown in Fig. 17 as a function of the rotation angle $\phi = \theta - \theta_0$ around **b** or **c**. θ_0 is an offset angle which depend on the orientation of the spherically shaped sample when inserted into the cryostat. As expected, within uncertainty, the background signal shows no angular dependence. The first signal labeled ν_1 shows a relatively small and negative frequency shift, whereas the second one, labeled ν_2, is large and positive. As demonstrated by the solid curves in Fig. 17, the angular dependence of these two signals is described very well by the function given in Eq. (A10). The values for the parameters $\nu_{0,i}$ and $\Delta\nu_i$ can be found in Table III.

It should be mentioned that, for both angular scans, the values for the initial asymmetry a_1 are always somewhat larger than those for a_2 (~ 0.12 vs ~ 0.10). As explained in Appendix A, the observed squared-cosine law means that

$$C_i^{ba}(\mathbf{q} = \mathbf{0}) = C_i^{ca}(\mathbf{q} = \mathbf{0}) = 0 \qquad \text{(B2)}$$

for site $i=1$ and $i=2$. Therefore, from an inspection of Table II, we deduce that the muons cannot be localized at sites 4e or 4f.

In addition to the two angular scans, three temperature scans have been performed with $\mathbf{B}_{\mathrm{ext}}$ parallel either to **a**, **b**, or **c**. In the upper panel of Fig. 18 the two Knight shifts $K_{\mathrm{ex},i}^{a}$ ($i=1$ and $i=2$) measured with $\mathbf{B}_{\mathrm{ext}} \| \mathbf{a}$ are presented as a function of the bulk susceptibility χ^a (a Clogston-Jaccarino plot). As in the case of the angular scans, a_1 is slightly larger than a_2, which indicates a larger muon population ($\sim 55\%$) for site 1 than for site 2 ($\sim 45\%$). The two solid lines represent linear fits to the data. It is seen that this yields a good description for both signals. This is consistent with expectation; see Eq. (A5). The two parameters obtained from each fit are listed in Table IV.

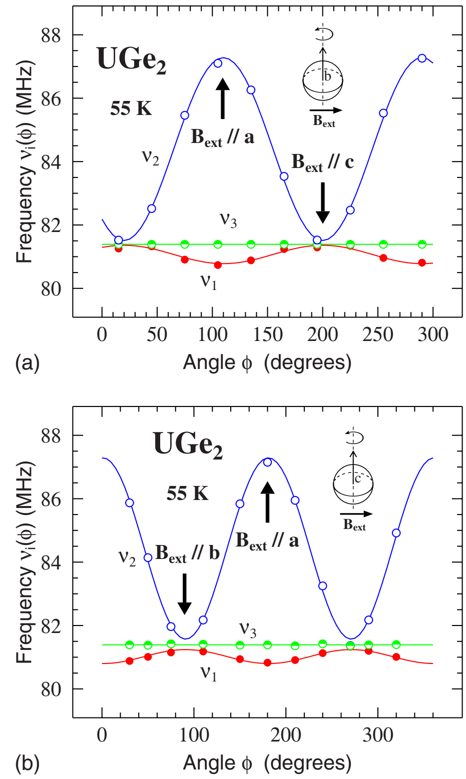

FIG. 17. (Color online) Angular dependence of the muon frequencies at 55 K. A sphere of single-crystalline UGe_2 was rotated around the **b** and **c** axes (upper and lower panel, respectively) in a field of $B_{\mathrm{ext}} = 0.6$ T perpendicular to the rotation axis. The solid lines for $\nu_1(\phi)$ and $\nu_2(\phi)$ are the results of fits to Eq. (A10). The error bars for the frequencies are within the symbol size. The background signal at $\nu_{BG} = 81.39$ MHz is shown as well. It is well described by a straight horizontal solid line in the two panels.

In the lower two panels of Fig. 18 the Knight shifts measured with $\mathbf{B}_{\mathrm{ext}} \| \mathbf{b}$ and $\mathbf{B}_{\mathrm{ext}} \| \mathbf{c}$ are displayed as a function of the bulk susceptibilities χ^b and χ^c, respectively. We have identified which curve stems from which muon site using the asymmetries as a fingerprint. As in all previous cases, a_1 is slightly larger than a_2.

Comparing the horizontal (χ^α) and vertical ($K_{\mathrm{ext}}^{\alpha}$) scales in Fig. 18, it is clearly seen that there is a 2 orders of magnitude difference between the values for $\mathbf{B}_{\mathrm{ext}} \| \mathbf{b}$ and $\mathbf{B}_{\mathrm{ext}} \| \mathbf{c}$ on the one hand, and $\mathbf{B}_{\mathrm{ext}} \| \mathbf{a}$ on the other hand. The small values for $\mathbf{B}_{\mathrm{ext}} \| \mathbf{b}$ and $\mathbf{B}_{\mathrm{ext}} \| \mathbf{c}$ make it difficult to obtain an accurate determination of the Knight shift.

The sharp drop of $|K_{\mathrm{ext},i}^{b}|$ for low values of χ^b probably indicates the start of muon diffusion. This happens at tem-

TABLE III. Fitted values for $\nu_{0,i}$ and $\Delta\nu_i$ found from the two angular scans for the two muon sites. The parameters are defined by Eq. (A10).

	rotation around **b** axis		rotation around **c** axis	
	$i=1$	$i=2$	$i=1$	$i=2$
$\nu_{0,i}$ (MHz)	81.36(2)	81.51(4)	81.24(3)	81.57(4)
$\Delta\nu_i$ (MHz)	−0.58(4)	5.77(6)	−0.44(5)	5.72(6)

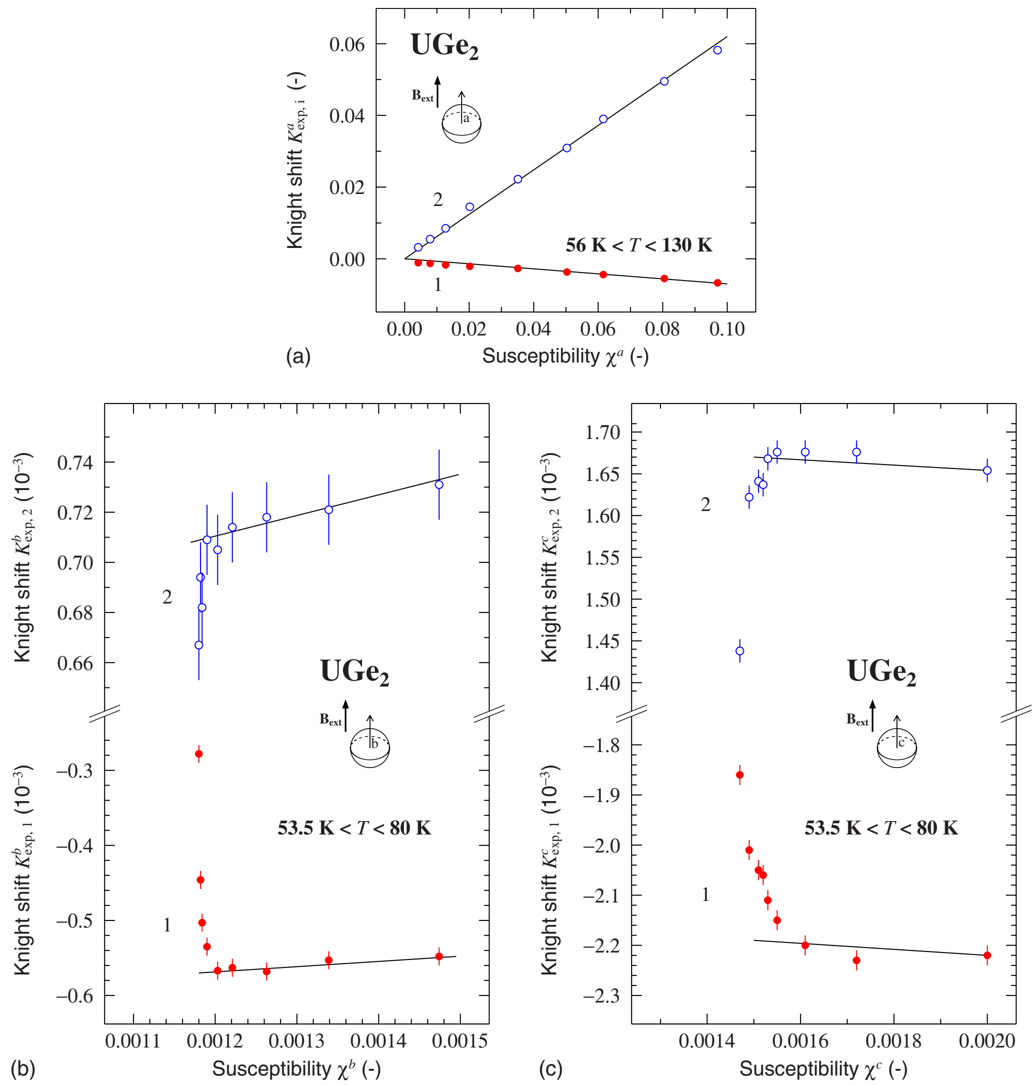

FIG. 18. (Color online) Clogston-Jaccarino plot of the muon Knight shift for $\mathbf{B}_{ext} \| \alpha$ (where $\alpha = \mathbf{a}, \mathbf{b}, \mathbf{c}$) as a function of the bulk magnetic susceptibility χ^α for the two muon localization sites. The muon Knight shift $K^\alpha_{exp,i}$ is plotted versus χ^α with the temperature as an implicit parameter. Both types of quantities were measured in a magnetic field of $B_{ext} = 0.6$ T and on the same spherically shaped sample and for each direction of $\mathbf{B}_{ext}$ at the same temperatures. The solid lines result from linear fits.

peratures $T > 66$ K. For $\mathbf{B}_{ext} \| \mathbf{c}$ it is less clear at which temperature the muon starts to diffuse. We shall take the reasonable hypothesis that for both directions of $\mathbf{B}_{ext}$ the muon starts to diffuse through the sample at the same temperature. Therefore, the data points for $T > 66$ K were not taken into account when fitting the data. In Fig. 18 the linear fits are shown and the fit parameters are given in Table IV. The larger error bars for $K^c_{exp,i}$ compared to $K^b_{exp,i}$ are caused by the difference in the number of data points that could be used in the fit.

We know from the Knight shift studies that we have to deal with two muon sites, at least for $T \gtrsim 55$ K. Information on the muon sites can be obtained also from the measured spontaneous fields. In Fig. 19 we display two zero-field spectra recorded at low temperature. Depending on the orientation of the initial polarization of the muon beam relative to the crystal axes, we observe either the sum of two damped oscillations which account for the whole available initial asymmetry, or a simple relaxing signal with the expected asymmetry. This means that two spontaneous local fields are probed and they are parallel to the **a** axis. This can only be possible if the conditions specified by Eq. (B2) apply. From the two measured spontaneous frequencies at 1.6 K, which is far below T_C, we can estimate the saturated values of the two spontaneous fields. We obtain $B^a_{0,1} = 62.90(4)$ mT and $B^a_{0,2} = 361.79(7)$ mT. As for the paramagnetic state, their values have been attributed to the sites with the help of the initial asymmetries. Their ratio is still $a_1/a_2 \simeq 55/45$.

We now discuss the Knight shift data and the values of the two spontaneous fields with the purpose to determine the two muon positions in UGe$_2$. Assuming the two hyperfine tensors to be scalar, i.e., $\mathfrak{H}^{aa}_i = \mathfrak{H}^{bb}_i = \mathfrak{H}^{cc}_i \equiv \mathfrak{H}_i$, from the measured values of $\mathcal{F}^{\alpha\alpha}_i$ (see Table IV) and Eq. (A7), we determine $\mathfrak{H}_i$ and therefore the tensor elements $C^{\alpha\alpha}_i(\mathbf{q}=\mathbf{0})$ using Eq. (A6). The results of these numerics are listed for both sites in Table IV. Comparing the three tensor elements $C^{\alpha\alpha}_1(\mathbf{q}=\mathbf{0})$ of Table IV with the results of the computation of these elements for different positions in Table II, we attribute the first measured

TABLE IV. Parameters deduced from the Clogston-Jaccarino plots and the coupling constants inferred from these parameters for the two muon sites, S_1 and S_2, in UGe_2. The hyperfine tensor is supposed to be scalar with its elements written as $\mathfrak{H}_i$.

	Quantities	**a** axis	**b** axis	**c** axis
S_1	$\mathcal{F}_1^{\alpha\alpha}$	−0.062(1)	0.074(21)	−0.080(37)
	$K_{\mathrm{cond},1}$	−0.00080(3)	−0.00066(7)	−0.00207(1)
	$\mathfrak{H}_1$	−0.023(14)	−0.023(14)	−0.023(14)
	$C_1^{\alpha\alpha}(\mathbf{q}=\mathbf{0})$	0.294(14)	0.430(25)	0.276(40)
S_2	$\mathcal{F}_2^{\alpha\alpha}$	0.591(4)	0.081(17)	−0.040(25)
	$K_{\mathrm{cond},2}$	0.0010(2)	0.00061(2)	0.00174(4)
	$\mathfrak{H}_2$	0.211(10)	0.211(10)	0.211(10)
	$C_2^{\alpha\alpha}(\mathbf{q}=\mathbf{0})$	0.713(11)	0.203(20)	0.082(27)

muon signal to muons at position 2b. Unfortunately, the measured three tensor elements $C_2^{\alpha\alpha}(\mathbf{q}=\mathbf{0})$ are not in agreement with any of the predictions for a high-symmetric interstitial position.

Using the measured $B_{0,1}^a$ value, we can check the assignment of the muon site labeled 1 as arising from position 2b and also gauge the hypothesis of a scalar hyperfine tensor. From the computed value of $C^{aa}(\mathbf{q}=0)$ for site 2b, see Table II, and Eq. (A3), we compute $\mathfrak{H}_1^{aa}=-0.025$. Taking the hyperfine tensor to be scalar, we should have $\Sigma_\alpha \mathfrak{H}_1^{\alpha\alpha}=-0.075$. We compute $\Sigma_\alpha \mathcal{F}_1^{\alpha\alpha}=-0.068$. Hence the condition given by Eq. (A7) does not seem to be satisfied. However, while the uncertainty on $\Sigma_\alpha \mathfrak{H}_1^{aa}$ is very small because it derives directly from the value of the low frequency which is well determined, the uncertainty on $\Sigma_\alpha \mathcal{F}_1^{\alpha\alpha}$ is large. Hence, the condition given by Eq. (A7) is in fact fairly well obeyed. Therefore the scalar hypothesis is supported by the numerics. Inspecting the uranium environment of the muon at position

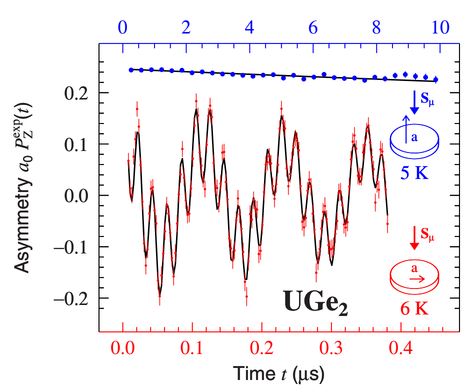

FIG. 19. (Color online) Examples of zero-field μSR spectra recorded at ambient pressure and low temperature for $\mathbf{S}_\mu \perp \mathbf{a}$ and $\mathbf{S}_\mu \parallel \mathbf{a}$ at the GPS and MuSR (Ref. 4) spectrometers, respectively. The initial asymmetry for the two measurements were a little different: $a_0=0.212$ and $0.196+0.050=0.246$ (the 0.050 asymmetry stems from the background contribution at μSR because of the relatively large muon beam cross section; such a contribution does not exist at GPS), respectively. This explains that the sum of the two amplitudes of the oscillations is not exactly equal to expectation if one looks at the spectrum recorded for $\mathbf{S}_\mu \parallel \mathbf{a}$ for reference. Note the two different horizontal time scales.

TABLE V. Estimated hyperfine constants for high-symmetry muon sites. The hyperfine tensor is assumed to be axial, with the axial axis parallel to the **b** crystal direction. For the 4j site we present the results for three possible values of the reduced coordinate y since the dipole tensor elements are strongly dependent on it; see Table II.

	Hyperfine constants	
Site	$\mathfrak{H}_i^{b^\perp}$	$\mathfrak{H}_i^{b^\parallel}$
2b $(0,\frac{1}{2},0)$	−0.025(0)	−0.018(11)
2d $(\frac{1}{2},\frac{1}{2},\frac{1}{2})$	2.05(0)	−3.5(1.7)
4i (0,0.1590,0)	2.05(0)	−3.5(1.7)
4j $(\frac{1}{2},0.1916,\frac{1}{2})$	−0.219(0)	1.1(5)
4j $(\frac{1}{2},0.1714,\frac{1}{2})$	−0.691(0)	2.0(9)
4j $(\frac{1}{2},0.1415,\frac{1}{2})$	−1.133(0)	2.9(1.3)

2b (see Fig. 1), we find there are eight nearest-neighbor uranium atoms to a muon, located at the corners of a rectangular parallelepiped, the muon being at the center of this structure. Perpendicular to **b** the basis is almost a square. This suggests that two elements of the hyperfine tensor are equal. With this physical insight, the two equal hyperfine constants for the basal plane, $\mathfrak{H}_{2\mathrm{b}}^{b^\perp}$, can be deduced directly from the measured spontaneous field. Using Eq. (A7), the value of $\mathfrak{H}_{2\mathrm{b}}^{b^\perp}$ just derived and data from Table IV, the other hyperfine constant, $\mathfrak{H}_{2\mathrm{b}}^{b^\parallel}$, is computed. The results are listed in Table V. As expected, the anisotropy of the hyperfine tensor is small, if any.

We now consider the other muon site. Proceeding with the same methodology as for the muon at site 2b, we have computed the hyperfine constants for the remaining three high-symmetry muon localization sites. The hyperfine constants are listed in Table V. While $\mathfrak{H}_{2\mathrm{d}}^{b^\perp}$ and $\mathfrak{H}_{4\mathrm{i}}^{b^\perp}$ are found to be positive with a value of ~ 2, $\mathfrak{H}_{4\mathrm{j}}^{b^\perp}$ is negative for the three y values. All the hyperfine constants determined up to now have always been found to be negative with an absolute value smaller than one. We refer to the data for Fe, Co, Ni, Gd, Dy,[38] and $DyNi_5$.[58] This corresponds to an hyperfine field antiparallel to the bulk magnetization. It suggests that the second muon site is at position 4j; see Fig. 1. On the other hand, $\mathfrak{H}_{4\mathrm{j}}^{b^\parallel}$ is clearly estimated to be positive. This seems to be inconsistent with our site assignment. However, we argue in Sec. IV B 1 that the hyperfine coupling tensor changes between the WP and SP phases. This means that, while the estimated value for $\mathfrak{H}_{4\mathrm{j}}^{b^\perp}$ is reliable since it derives directly from the second measured spontaneous field at low temperature, our computed value for $\mathfrak{H}_{4\mathrm{j}}^{b^\parallel}$ may not be correct. The reason is simply that we use the paramagnetic Knight shift data in combination with the sum rule of Eq. (A7). Because of lack of sufficient information, we will not discuss any further the muon site assignment. No matter the restricted amount of information extracted from the measurements on the coupling constants, the comparison of the $\mathfrak{H}_{2\mathrm{d}}^{b^\perp}$ and $\mathfrak{H}_{4\mathrm{j}}^{b^\perp}$ values is quite interesting. The coupling constant $\mathfrak{H}_{2\mathrm{d}}^{b^\perp}$ is particularly small and the ratio $\mathfrak{H}_{4\mathrm{j}}^{b^\perp}/\mathfrak{H}_{2\mathrm{d}}^{b^\perp}$ is quite large, at least 8.8. This is a key reliable characteristics which is used in Sec. IV B.

As explained in Appendix A, the amplitude and the level of the oscillation observed when performing an angular scan may provide information on the coupling constants. From Eq. (A11) and the discussion leading to these results, we derive

$$\nu_{0,i} = \nu_{\rm BG}(1 + \mathcal{F}_i^{aa}\chi^a),$$

$$\Delta\nu_i = \nu_{\rm BG}(\mathcal{F}_i^{cc}\chi^c - \mathcal{F}_i^{aa}\chi^a) \tag{B3}$$

for the sphere rotated around the **b** and

$$\nu_{0,i} = \nu_{\rm BG}(1 + \mathcal{F}_i^{bb}\chi^b),$$

$$\Delta\nu_i = \nu_{\rm BG}(\mathcal{F}_i^{aa}\chi^a - \mathcal{F}_i^{bb}\chi^b), \tag{B4}$$

when **c** is the rotation axis. We use $\nu_{\rm BG}$ rather than $\nu_{\rm ext}$ to take into account that the effective field on the sample was slightly shifted. $\mathcal{F}_i^{aa}$ can be estimated directly from the first equation in Eq. (B3)

$$\mathcal{F}_i^{aa} = \frac{1}{\chi^a}\left(\frac{\nu_{0,i}}{\nu_{\rm BG}} - 1\right). \tag{B5}$$

Since $\chi^a(T{=}55\ \text{K}){=}1.32\times10^{-1}$, we compute for example $\mathcal{F}_2^{aa}{=}0.012(4)$. This is clearly not consistent with the value deduced from the Clogston-Jaccarino plot [$\mathcal{F}_2^{aa}{=}0.591(4)$, see Table IV]. In the same way, using $\chi^b(T{=}55\ \text{K}){=}1.32\times10^{-3}$, we compute, for example, $\mathcal{F}_1^{bb}{=}-1.39(27)$ whereas we were expecting $\mathcal{F}_1^{bb}{=}0.074(21)$, see Table IV. Therefore our measurements for the two sites are not in agreement with the predictions given at Eq. (A9) but the data still follow the law written in Eq. (A8). Basically this law can be seen as a direct consequence of the high symmetry at the muon site. However, the specific model used to derive Eq. (A9) neglects the spin-orbit interaction of the uranium electrons.[59] This is certainly not a good approximation for an uranium compound.

Finally, we note that the multiplicity at position 4j is twice as much than at position 2b; see Fig. 1. This fact cannot be used as an argument to reject the 4j assignment as a possibility since the probability for trapping of a muon in a site is obviously not determined by its multiplicity. Since we have just assigned the two measured muon signals to two positions in the crystal structure, in the main text the two sites are labeled using the Wyckoff notation.

[1] S. S. Saxena, P. Agarwal, K. Ahilan, F. M. Grosche, R. K. W. Haselwimmer, M. J. Steiner, E. Pugh, I. R. Walker, S. R. Julian, P. Monthoux, G. G. Lonzarich, A. Huxley, I. Sheikin, D. Braithwaite, and J. Flouquet, Nature (London) **406**, 587 (2000).

[2] K. Satoh, S. W. Yun, I. Ukon, I. Umehara, Y. Ōnuki, H. Aoki, S. Uji, T. Shimizu, I. Sakamoto, M. Hunt, P. Meeson, P-A. Probst, and M. Springford, J. Magn. Magn. Mater. **104-107**, 39 (1992).

[3] A. Huxley, I. Sheikin, E. Ressouche, N. Kernavanois, D. Braithwaite, R. Calemczuk, and J. Flouquet, Phys. Rev. B **63**, 144519 (2001).

[4] A. Yaouanc, P. Dalmas de Réotier, P. C. M. Gubbens, C. T. Kaiser, A. A. Menovsky, M. Mihalik, and S. P. Cottrell, Phys. Rev. Lett. **89**, 147001 (2002).

[5] P. Boulet, A. Daoudi, M. Potel, H. Noël, G. M. Gross, G. André, and F. Bourée, J. Alloys Comp. **247**, 104 (1997).

[6] K. Oikawa, T. Kamiyama, H. Asano, Y. Ōnuki, and M. Kohgi, J. Phys. Soc. Jpn. **65**, 3229 (1996).

[7] D. Aoki, A. Huxley, E. Ressouche, I. Sheikin, J. Flouquet, J. P. Brison, and C. Paulsen, J. Phys. Chem. Solids **63**, 1179 (2002).

[8] H. H. Hill, *Plutonium 1970 and Other Actinides* (AIME, New York, 1970).

[9] N. Kernavanois, B. Grenier, A. Huxley, E. Ressouche, J. P. Sanchez, and J. Flouquet, Phys. Rev. B **64**, 174509 (2001).

[10] Y. Ōnuki, I. Ukon, S. W. Yun, I. Umehara, K. Satoh, T. Fukuhara, H. Sato, S. Takayanagi, M. Shikama, and A. Ochiai, J. Phys. Soc. Jpn. **61**, 293 (1992).

[11] C. Pfleiderer and A. D. Huxley, Phys. Rev. Lett. **89**, 147005 (2002).

[12] A. Huxley, E. Ressouche, B. Grenier, D. Aoki, J. Flouquet, and C. Pfleiderer, J. Phys.: Condens. Matter **15**, S1945 (2003).

[13] N. Tateiwa, T. C. Kobayashi, K. Amaya, Y. Haga, R. Settai, and Y. Ōnuki, Phys. Rev. B **69**, 180513(R) (2004).

[14] A. Huxley, I. Sheikin, and D. Braithwaite, Physica B **284-288**, 1277 (2000).

[15] S. Watanabe and K. Miyake, J. Phys. Soc. Jpn. **71**, 2489 (2002).

[16] T. C. Kobayashi, K. Hanazono, N. Tateiwa, K. Amaya, Y. Haga, R. Settai, and Y. Onuki, J. Phys.: Condens. Matter **14**, 10779 (2002).

[17] Y. Haga, M. Nakashima, R. Settai, S. Ikeda, T. Okubi, S. Araki, T. C. Kobayashi, N. Tateiwa, and Y. Onuki, J. Phys.: Condens. Matter **14**, L125 (2002).

[18] N. Tateiwa, K. Hanazono, T. C. Kobayashi, K. Amaya, T. Inoue, K. Kindo, Y. Koike, N. Metoki, Y. Haga, R. Settai, and Y. Ōnuki, J. Phys. Soc. Jpn. **70**, 2876 (2001).

[19] Y. Kitaoka, H. Kotegawa, A. Harada, S. Kawasaki, Y. Kawasaki, Y. Haga, E. Yamamoto, Y. Ōnuki, K. M. Itoh, E. E. Haller, and H. Harima, J. Phys.: Condens. Matter **17**, S975 (2005).

[20] N. Tateiwa, T. C. Kobayashi, K. Hanazono, K. Amaya, Y. Haga, R. Settai, and Y. Onuki, J. Phys.: Condens. Matter **13**, L17 (2001).

[21] A. Jacko, J. Fjærestad, and B. Powell, Nat. Phys. **5**, 422 (2009).

[22] T. Terashima, T. Matsumoto, C. Terakura, S. Uji, N. Kimura, M. Endo, T. Komatsubara, and H. Aoki, Phys. Rev. Lett. **87**, 166401 (2001).

[23] V. H. Tran, S. Paschen, R. Troć, M. Baenitz, and F. Steglich, Phys. Rev. B **69**, 195314 (2004).

[24] R. Caspary, P. Hellmann, M. Keller, G. Sparn, C. Wassilew, R. Köhler, C. Geibel, C. Schank, F. Steglich, and N. E. Phillips, Phys. Rev. Lett. **71**, 2146 (1993).

[25] R. Feyerherm, A. Amato, F. N. Gygax, A. Schenck, C. Geibel, F. Steglich, N. Sato, and T. Komatsubara, Phys. Rev. Lett. **73**, 1849 (1994).

[26] M. Kyogaku, Y. Kitaoka, K. Asayama, C. Geibel, C. Schank, and F. Steglich, J. Phys. Soc. Jpn. **62**, 4016 (1993).
[27] K. Kuwahara, K. Kuwahara, H. Sagayama, K. Iwasa, M. Kohgi, Y. H. Y. Ōnuki, K. Kakurai, M. Nishi, K. Nakajima, N. Aso, and Y. Uwatoko, Physica B **312-313**, 106 (2002).
[28] M. P. Marder, *Condensed Matter Physics* (John Wiley & Sons, New York, 2000).
[29] S. Suzuki, S. Sato, T. Ejima, K. Murata, Y. Kudo, T. Takahash, T. Komatsubara, N. Sato, M. Kasaya, T. Suzuki, T. Kasuya, S. Suga, H. Matsubara, Y. Saito, A. Kimura, K. Soda, Y. Ōnuki, T. Mori, A. Kakizaki, and T. Ishii, Jpn. J. Appl. Phys. **8**, 59 (1993).
[30] M. Biasini and R. Troc, Phys. Rev. B **68**, 245118 (2003).
[31] A. N. Yaresko, P. Dalmas de Réotier, A. Yaouanc, N. Kernavanois, J.-P. Sanchez, A. A. Menovsky, and V. N. Antonov, J. Phys.: Condens. Matter **17**, 2443 (2005).
[32] A. B. Shick and W. E. Pickett, Phys. Rev. Lett. **86**, 300 (2001).
[33] P. Dalmas de Réotier and A. Yaouanc, J. Phys.: Condens. Matter **9**, 9113 (1997).
[34] A. Amato, Rev. Mod. Phys. **69**, 1119 (1997).
[35] D. Andreica, Ph.D. thesis, ETH Zürich, 2001.
[36] K. Nishiyama, S. W. Nishiyama, and W. Higemoto, Physica B **326**, 41 (2003).
[37] A. Eiling and J. Schilling, J. Phys. F: Met. Phys. **11**, 623 (1981).
[38] A. B. Denison, H. Graf, W. Kündig, and P. F. Meier, Helv. Phys. Acta **52**, 460 (1979).
[39] N. Nishida, K. Nagamine, R. S. Hayano, T. Yamazaki, D. G. Fleming, R. A. Duncan, J. H. Brewer, A. Ahktar, and H. Yasuoka, J. Phys. Soc. Jpn. **44**, 1131 (1978).
[40] S. Estreicher and P. F. Meier, Phys. Rev. B **25**, 297 (1982).
[41] P. Meier, in *Muons and Pions in Materials Research*, edited by J. Chappert and R. I. Grynszpan (North-Holland, Amsterdam, 1984).
[42] S. Sakarya, Ph.D. thesis, Technical University Delft, 2007.
[43] P. C. M. Gubbens, P. Dalmas de Réotier, A. Yaouanc, A. A. Menovsky, and C. E. Snel, Hyperfine Interact. **85**, 245 (1994).
[44] A. Yaouanc, P. Dalmas de Réotier, and E. Frey, Phys. Rev. B **47**, 796 (1993).
[45] S. Henneberger, E. Frey, P. G. Maier, F. Schwabl, and G. M. Kalvius, Phys. Rev. B **60**, 9630 (1999).
[46] A. Yaouanc, P. Dalmas de Réotier, P. C. M. Gubbens, A. M. Mulders, F. E. Kayzel, and J. J. M. Franse, Phys. Rev. B **53**, 350 (1996).
[47] G. G. Lonzarich and L. Taillefer, J. Phys. C **18**, 4339 (1985).
[48] N. R. Bernhoeft and G. G. Lonzarich, J. Phys.: Condens. Matter **7**, 7325 (1995).
[49] A. de Visser, N. T. Huy, A. Gasparini, D. E. de Nijs, D. Andreica, C. Baines, and A. Amato, Phys. Rev. Lett. **102**, 167003 (2009).
[50] N. J. Curro, T. Caldwell, E. D. Bauer, L. A. Morales, M. J. Graf, Y. Bang, A. V. Balatsky, J. D. Thompson, and J. L. Sarrao, Nature (London) **434**, 622 (2005).
[51] M. Wulff, G. H. Lander, B. Lebech, and A. Delapalme, Phys. Rev. B **39**, 4719 (1989).
[52] E. Runge, P. Fulde, D. V. Efremov, N. Hasselmann, and G. Zwicknagl, Phys. Rev. B **69**, 155110 (2004).
[53] A. Yaouanc, P. Dalmas de Réotier, and E. H. Brandt, Phys. Rev. B **55**, 11107 (1997).
[54] A. Schenck and F. N. Gygax, in *Handbook of magnetic Materials*, edited by K. H. J. Buschow (Elsevier, Amsterdam, 1995), Vol. 9.
[55] J. Jensen and A. R. Mackintosh, *Rare Earth Magnetism: Structures and Excitations* (Clarendon, Oxford, 1991).
[56] A. Schenck, in *Muon Science: Muons in Physics, Chemistry and Materials*, edited by S. Lee, S. H. Kilcoyne, and R. Cywinski (Institute of Physics, Bristol, 1999).
[57] P. Dalmas de Réotier, A. Yaouanc, and E. Frey, Phys. Rev. B **50**, 3033 (1994).
[58] A. M. Mulders, C. T. Kaiser, S. J. Harker, P. C. M. Gubbens, A. Amato, F. N. Gygax, A. Schenck, P. Dalmas de Réotier, A. Yaouanc, K. H. J. Buschow, and A. A. Menovsky, Phys. Rev. B **67**, 014303 (2003).
[59] G. C. Carter, L. H. Bennett, and D. J. Kahan, *Metallic Shifts in NMR, Part I* (Pergamon, Oxford, 1977).